J. Fluid Mech. (1996), *vol.* 329, *pp.* 155–186

A numerical study of the rheological properties of suspensions of rigid, non-Brownian fibres

By MICHAEL B. MACKAPLOW† AND ERIC S. G. SHAQFEH

Department of Chemical Engineering, Stanford University, Stanford, CA 94305-5025, USA

(Received 30 January 1995 and in revised form 20 June 1996)

Using techniques developed in our previous publication (Mackaplow *et al.* 1994), we complete a comprehensive set of numerical simulations of the volume-averaged stress tensor in a suspension of rigid, non-Brownian slender fibres at zero Reynolds number. In our problem formulation, we use slender-body theory to develop a set of integral equations to describe the interfibre hydrodynamic interactions at all orders. These integral equations are solved for a large number of interacting fibres in a periodically extended box. The simulations thus developed are an accurate representation of the suspensions at concentrations up to and including the *semi-dilute* regime. Thus, large changes in the suspensions properties can be obtained. The rheological properties of suspensions with concentrations ranging from the dilute regime, through the dilute/semi-dilute transition, and into the semi-dilute regime, are surprisingly well predicted by a dilute theory that takes into account two-body interactions. The accuracy of our simulations is verified by their ability to reproduce published suspension extensional and shear viscosity data for a variety of fibre aspect ratios and orientation distributions, as well as a wide range of suspension concentrations.

1. Introduction

Suspensions of non-Brownian fibres in a Newtonian suspending fluid occur in many industrial applications, such as the production of fibre composites and the pumping of pulp slurries. Such suspensions often have complicated rheological properties that are quite different from those of the suspending fluid, even when the volume fraction of the fibres is very small. For example, a volume fraction of less than 1% can often increase the stress by an $O(1)$ amount beyond that of the fibre-free fluid. This has been observed experimentally in filament spinning (Mewis & Metzner 1974; Pittman & Bayram 1991), cup-and-plate rheometers (Bibbo 1987), and falling-ball rheometry (Milliken *et al.* 1989), to name but a few investigations. Mewis & Metzner (1974) observed values of the effective extensional viscosity which increased by a factor of 260 with the addition of a very small volume fraction ($< 1\%$) of high-aspect ratio fibres.

Fibre suspensions generally exhibit strongly non-Newtonian behaviour. This can be understood by noting that the volume-averaged deviatoric stress tensor, $\langle \boldsymbol{\sigma}^D \rangle$, in a

† Present address: Merck & Co. Inc., Merck Manufacturing Division, WP78-102, West Point, PA 19486-0004, USA.

fibre suspension can be written

$$\langle \boldsymbol{\sigma}^D \rangle = 2\mu \langle \mathbf{e} \rangle + n \langle \mathbf{S} \rangle \tag{1}$$

where μ is the viscosity of the suspending fluid, $\mathbf{e}$ is the volume-averaged fluid rate of strain tensor, n is the particle number density, and $\langle \mathbf{S} \rangle$ is the average particle 'stresslet'. The latter is a symmetric, traceless tensor that is a function of particle shapes, sizes, orientations, and centre-of-mass distributions. It will be discussed in more detail in §2. In general, for orientable particles, $\langle \mathbf{S} \rangle$ will not have the same tensorial form as $\langle \mathbf{e} \rangle$. Therefore, the volume-averaged deviatoric stress tensor of the suspension cannot be written merely as $2\mu_{eff} \langle \mathbf{e} \rangle$, where μ_{eff} is referred to as the effective viscosity of the suspension.

In addition, the rheological properties of fibre suspensions may change dramatically during startup. This is because the instantaneous suspension properties are a strong function of the fibre orientation distribution. The orientation distribution evolves over time as particles rotate in the mean flow and interact with each other until a steady-state distribution is reached. This has been observed experimentally by Bibbo (1987). In industrial applications, such as the injection moulding of suspensions, it is possible that the suspension will experience a rapidly changing flow field such that a steady-state orientation distribution will never be reached. Thus, it is important to understand both the development of the orientation distribution and how the rheological properties vary as a function of it. We note that the effect of the particle orientation distribution on the rheological properties of the suspension is particularly important for large particle aspect ratios, as indicated by equation (11) below.

The reason that small volume fractions of fibres can have such large effects on the rheological properties of a suspension can be understood by examining the theoretical results of Batchelor (1970) for isolated fibres, henceforth referred to as the *dilute theory*. These show that the disturbance to the flow field created by a fibre of aspect ratio A is only $1/\ln(2A)$ weaker than a sphere having the same diameter as the fibre length. Moreover, the disturbance extends over the same fluid volume. Thus, the disturbance per unit particle volume created by a fibre relative to that of a sphere is $O(A^2/\ln(A))$, which can be quite large even with fibres of moderate aspect ratio. However, only the governing equations for suspensions where the fibres are not interacting with each other are analytically tractable. Since, as shown by the dilute theory, the interaction length of a fibre is determined by its physical length, $2l$, fibre interactions can only be neglected when $nl^3 \ll 1$. This is a much more restrictive condition than requiring that the volume fraction of inclusions, $\phi \ll 1$, and the concentration regime where $nl^3 \ll 1$ is referred to as the *dilute* regime. $O(1)$ property changes cannot be obtained in the dilute regime. Thus, the consideration of any suspension sufficiently concentrated to be of practical importance must include fibre–fibre interactions.

In his theoretical study of rigid fibres aligned in a viscous flow, Batchelor (1971) investigated suspension concentrations up to semi-dilute. This is a concentration regime where the average interfibre spacing is much less than the characteristic fibre length, l. Thus there are many fibre–fibre interactions. However, the average closest approach distance of any two fibres is much greater than the characteristic fibre width, b. To account for fibre–fibre interactions, Batchelor (1971) used a type of cell model which assumes that the disturbance created by a fibre would decay, or be 'screened', on a length of the order of the average interfibre spacing. Dinh & Armstrong (1984) extended this approach to determine the evolution of the orientation distributions, and thus also the evolution of the stress tensor, in suspensions having arbitrary

initial orientation distributions. They postulated that the closest approach distance determined the screening length, so that the screening length would differ for aligned and isotropic suspensions. Pittman & Bayram (1990) later extended the approach of Batchelor (1971) to polydisperse suspensions.

In their theoretical study, Shaqfeh & Fredrickson (1990) investigated the low-Reynolds number hydrodynamic stress in fibre suspensions. They considered suspensions concentrations up to semi-dilute and used multiple scattering to sum various classes of fibre–fibre interactions. The screening length, χ, in the suspension was found to be

$$\chi = b\left[\frac{\hat{C}}{\phi}\ln\frac{1}{\phi}\times\left(1+O\left(1\Big/\ln\frac{1}{\phi}\right)\right)\right]^{1/2}$$

where $\hat{C}$ is a constant that depends on the fibre shape and orientation distribution. If we neglect the weak $\ln(1/\phi)$ part of this expression, this result reduces to the same suspension screening length that was originally assumed by Batchelor (1971). However, the result of Shaqfeh & Fredrickson (1990) exactly specifies $\hat{C}$. It is of particular interest that this scaling is predicted not only for the aligned suspensions considered by Batchelor (1971), but for isotropic suspensions also. Although the average interfibre spacing is approximately the same for both aligned and isotropic suspensions, the average distance of closest approach is not.

Claeys & Brady (1993) have investigated the properties of suspensions of prolate spheroids in low-Reynolds-number flow using Stokesian dynamics numerical simulations. This technique can be used to simulate suspensions at all particle volume fractions, since the close particle–particle interactions that are present at higher suspension concentrations are specifically accounted for through the lubrication forces. However, although they have considered aspect ratios up to 50, their system of equations and unknowns becomes increasingly ill-conditioned as the fibre aspect ratio increases. They noted the surprising result that for isotropic suspensions of aspect ratio 50 particles, their simulations showed no evidence of particle interactions for suspension concentrations up to $nl^3 \approx 6$, even though one expects particle interactions to have a noticeable effect at such concentrations. Their simulations did show such effects for similar values of nl^3 but only for smaller aspect ratio particles.

From the foregoing discussion, we see that most previous theoretical predictions of the rheological properties of fibre suspensions have relied on cell models. These require an *ad hoc* choice of cell size. The much more rigorous analysis of Shaqfeh & Fredrickson (1990) includes only the summation of certain subclasses of fibre interactions. Experimentally, it is difficult to get detailed insight into suspension rheology, since it is not possible to methodically vary the orientation distribution and simultaneously measure all of the components of the stress tensor. Finally, it appears that it is difficult for Stokesian dynamics simulations to capture the effect of particle interactions for large aspect ratio particles.

In §2 we formulate a set of integral equations which can be solved to yield the full volume-averaged stress tensor for a suspension of rigid fibres in a Newtonian fluid. Model suspensions are generated by periodically replicating a finite number of fibres in a box throughout space. Slender-body theory is used to represent each fibre as a line distribution of Stokeslets along its axis. The Stokeslet distribution along each fibre axis is chosen to satisfy the appropriate boundary conditions on the surfaces of *all* of the fibres. This formulation explicitly considers all fibre–fibre interactions and is valid for all concentrations up to and including semi-dilute. In

addition, our formulation is valid for arbitrary orientation distributions and suffers no numerical difficulties at large aspect ratios. This approach is very similar to the one used by the present authors to study heat and mass transport in fibre suspensions (Mackaplow, Shaqfeh & Schiek 1994). In §3 we discuss our method of solving the resulting governing equations. In §4 we briefly review the existing theory for the rheology of suspensions of non-Brownian fibres in a Newtonian fluid.

In §5, we consider both aligned and isotropic fibre suspensions of concentrations $0.01 < nl^3 < 15$ in a uniaxial extensional flow. We find good agreement with the dilute theory for $nl^3 < 1$. Beyond the dilute regime, fibre–fibre interactions enhance the average particle stresslet significantly. Our results are consistent with the screening length of the suspension changing from depending on the fibre length in the dilute regime to on the average interfibre spacing in the semi-dilute regime. This is the first verification of this prediction of the semi-dilute theory as presented by Shaqfeh & Fredrickson (1990). The screening length scaling was found to occur for both aligned and isotropic semi-dilute suspensions, again as predicted by Shaqfeh & Fredrickson (1990). We also directly verify suspension screening by studying the decay of the velocity field created by individual stokeslets.

Also in §5, we compare our simulations to the experimental data of Weinberger (1970), Mewis & Metzner (1974), and Pittman & Bayram (1990), for aligned distributions, and Bibbo (1987), for both isotropic and steady-state shear distributions. We found excellent agreement between the experiments and simulations and further support for the concentration scaling of the screening noted above. Finally, in §6 we provide a concluding discussion of our simulation technique and reiterate the important results. We also discuss a straightforward extension of our technique to determine the effective mobility of fibres in a sedimenting suspension.

2. Mathematical formulation of the problem

We consider a suspension of rigid, non-Brownian particles in a Newtonian fluid. When the Reynolds number of the suspension is much less than unity, boundary integral methods can be used to represent the disturbance to the flow field due to the presence of the particles, $\boldsymbol{v}^D(\boldsymbol{x})$, as an integral of singularities distributed over the particle surfaces (Ladyzehnskaya 1963)

$$\boldsymbol{v}^D(\boldsymbol{x}) = \sum_{i=1}^{N} \left[\int_{\mathscr{A}_i} \boldsymbol{f}(\boldsymbol{x}') \cdot \boldsymbol{H}(\boldsymbol{x} - \boldsymbol{x}') \mathrm{d}\mathscr{A}_i(\boldsymbol{x}') \right]. \tag{2}$$

$\mathscr{A}_i$ denotes the surface of particle i, $\boldsymbol{f}(\boldsymbol{x})$ is the force/area the particle exerts on the fluid, and $\boldsymbol{H}(\boldsymbol{x})$ is the Oseen tensor, $(1/8\pi\mu)(\boldsymbol{\delta}/|\boldsymbol{x}| + \boldsymbol{x}\boldsymbol{x}/|\boldsymbol{x}|^3)$, which determines the response of a fluid to a point force. When combined with integral equations specifying the total net force and torque on each particle, the result is a coupled set of two-dimensional integral equations that can be solved numerically for the singularity distributions on, and velocities and angular velocities of, each particle. The former are related to the rheological properties of the suspension. In particular, the contribution of the particles to the deviatoric stress tensor, $\langle \boldsymbol{\sigma}^{(P)} \rangle$, is

$$\begin{aligned} \langle \boldsymbol{\sigma}^{(P)} \rangle &= -n \langle \boldsymbol{S} \rangle \\ &= -\tfrac{1}{2} n \left\langle \int_{\mathscr{A}_i} \left[(\boldsymbol{x}\boldsymbol{f}(\boldsymbol{x})) + (\boldsymbol{x}\boldsymbol{f}(\boldsymbol{x}))^T - \tfrac{2}{3}(\boldsymbol{\delta}\boldsymbol{x} \cdot \boldsymbol{f}(\boldsymbol{x})) \right] \mathrm{d}\mathscr{A}_i(\boldsymbol{x}) \right\rangle \end{aligned} \tag{3}$$

where $\langle \ldots \rangle$ denotes an average over all particles in the suspension.

The full boundary integral method approach, which was used by Youngren & Acrivos (1975) to study flow around isolated spheroids and cylinders, is valid for arbitrary particle shapes and concentrations. Unfortunately, such an approach is computationally intensive and impractical for more than a few particles. For fibres we can make this problem more amenable to numerical solution by using slender-body theory.

The basic idea is that to understand the behaviour of fibre suspensions one does not need to know the entire force/area distribution over the fibre surface. One only needs to know the integral of the force around the perimeter at a given axial position on the fibre, $\boldsymbol{F}(s)$. The slender-body theory approximation reduces (3) to

$$\begin{aligned}\langle \boldsymbol{\sigma}^{(P)} \rangle &= -n \langle \boldsymbol{S} \rangle \\ &= -\tfrac{1}{2} n \left\langle \int \left[(s\boldsymbol{p}\boldsymbol{F}(s)) + (s\boldsymbol{p}\boldsymbol{F}(s))^T - \tfrac{2}{3}(\boldsymbol{\delta} s\boldsymbol{p} \cdot \boldsymbol{F}(s)) \right] \mathrm{d}s \right\rangle \times \left(1 + O(A^{-1})\right) \quad (4)\end{aligned}$$

where $\boldsymbol{p}$ is the fibre orientation vector and A is the aspect ratio of the fibres. We will show that slender-body theory can be used to consider fibre suspensions at concentrations up through semi-dilute.

To develop the governing slender-body theory equations for fibre suspensions, we follow Batchelor (1970) and expand the one-fibre version of (2) about the major axis of the fibre

$$\boldsymbol{v}^D(\boldsymbol{x}) = \boldsymbol{v}(\boldsymbol{x}) - \boldsymbol{v}^\infty(\boldsymbol{x}) = \int \boldsymbol{F}(s) \cdot \boldsymbol{H}(\boldsymbol{x} - \boldsymbol{x}_c - s\boldsymbol{p}) \mathrm{d}s \times \left(1 + O(b/h)\right). \quad (5)$$

$\boldsymbol{x}_c$ and b denote the fibre centre position and its characteristic width, respectively; h is the distance from the major axis of the fibre; $\boldsymbol{v}^\infty(\boldsymbol{x})$ is the undisturbed velocity at $\boldsymbol{x}$. We have non-dimensionalized the velocities with $\dot{\gamma} l$, where $\dot{\gamma}$ is the mean shear rate in the suspension, $\boldsymbol{H}(\boldsymbol{x})$ with $1/(8\pi\mu l)$, and $\boldsymbol{F}(s)$ with $8\pi\mu\dot{\gamma} l$.

By definition, in the semi-dilute regime the average closest approach distance between any two fibres is much greater than b. Thus, most interfibre interactions at suspension concentrations up to and including semi-dilute can be well approximated by representing fibres as line distributions of Stokeslets. However, even at such concentrations, there is a finite probability of two fibres approaching within a distance of $O(b)$. In aligned suspensions, the probability of this is $O(\phi)$, and an $O(l)$ distance along each fibre will be involved. As discussed by Batchelor (1971), the effect of such a close interaction will be to reduce to the separation speed of the fibres to $\ll O(\dot{\gamma} l)$ and produce an $O(1)$ increase in the fibre stresslets. Thus, only an $O(\phi)$ error is introduced into the mean particle stresslet by neglecting such interactions.

A similar analysis can be performed for isotropic suspensions using the lubrication theory results of Claeys & Brady (1989). In contrast to aligned suspensions, when two fibres are 'close', they will be so only over an $O(b)$ distance along their axes. As a result, two fibres must approach much closer, within $O\left(\epsilon b \ln(1/\phi^{1/2})/A\right)$, where $\epsilon \ll 1$, before an $O(\dot{\gamma} l)$ decrease in separation speed and $O(1)$ increase in the stresslets results. (The above assumes suspension screening on the length scales derived by Shaqfeh & Fredrickson (1990). This will be proven *a posteriori* in §5). The probability of such a close approach is $O\left(\epsilon\phi \ln(1/\phi^{1/2})\right)$. Thus, again we expect the neglected close interactions in the semi-dilute regime to have a negligible effect on our results.

Returning to the derivation of the governing equation, following Batchelor (1970) we can relate $\boldsymbol{F}(s)$ to the undisturbed flow field experienced by the fibre, $\boldsymbol{v}^\infty(\boldsymbol{x})$, using

the method of matched asymptotic expansions. This yields an integral equation for $\boldsymbol{F}(s)$, namely

$$\boldsymbol{U} + [\boldsymbol{\Omega} \times s\boldsymbol{p}] - \boldsymbol{v}^{\infty}(\boldsymbol{x}_c + s\boldsymbol{p}) = 2\left(\ln 2A + \ln \frac{(1-s^2)^{1/2}}{\hat{b}(s)}\right)(\boldsymbol{\delta} + \boldsymbol{pp}) \cdot \boldsymbol{F}(s) + (\boldsymbol{\delta} - 3\boldsymbol{pp}) \cdot \boldsymbol{F}(s) + (\boldsymbol{\delta} + \boldsymbol{pp}) \cdot \int \frac{\boldsymbol{F}(s') - \boldsymbol{F}(s)}{|s - s'|} \mathrm{d}s'. \tag{6}$$

The velocity of the fibre and its angular velocity about its center are denoted by $\boldsymbol{U}$ and $\boldsymbol{\Omega}$, respectively. As shown by Batchelor (1970), $\hat{b}(s)$, which is non-dimensionalized by the characteristic fibre radius b, is related to the local perimeter of the fibre cross-section. For circular cross-sections, it is simply the local fibre radius. Equation (6) is valid for fibres whose cross-sections have a high degree of symmetry (see Batchelor 1970).

If other fibres are present in the suspension then we add their disturbance velocities to the right-hand side of (6) to describe the effect of the other axial singularity distributions on a given fibre. Note that the linearity of the creeping flow equations requires that the velocity evaluated on the surface of any fibre is just a superposition of the disturbance velocities created by all of the fibres plus the undisturbed velocity. The axial singularity distributions must be chosen such that the no-slip condition is satisfied on the surface of each of the N fibres. For fibre 'j' this yields

$$\boldsymbol{U}_j + \boldsymbol{\Omega}_j \times s\boldsymbol{p}_j = \boldsymbol{v}^{\infty}(\boldsymbol{x}_{cj} + s\boldsymbol{p}_j) + \sum_{\substack{i=1 \\ i \neq j}}^{N} \int \boldsymbol{H}(\boldsymbol{x}_{c_i} + s'\boldsymbol{p}_i - \boldsymbol{x}_{c_j} - s\boldsymbol{p}_j) \cdot \boldsymbol{F}_i(s') ds' + 2\left(\ln 2A + \ln \frac{(1-s^2)^{1/2}}{\hat{b}(s)}\right)(\boldsymbol{\delta} + \boldsymbol{p}_j\boldsymbol{p}_j) \cdot \boldsymbol{F}_j(s) + (\boldsymbol{\delta} - 3\boldsymbol{p}_j\boldsymbol{p}_j) \cdot \boldsymbol{F}_j(s) + (\boldsymbol{\delta} + \boldsymbol{p}_j\boldsymbol{p}_j) \cdot \int \frac{\boldsymbol{F}_j(s) - \boldsymbol{F}_j(s')}{|s - s'|} \mathrm{d}s', \quad j = 1, \ldots, N. \tag{7}$$

Combining (7) with

$$\int \boldsymbol{F}_j(s) \mathrm{d}s = 0, \tag{8}$$

$$\left[\int s\boldsymbol{F}_j(s) \mathrm{d}s\right] \times \vec{p}_j = 0, \quad j = 1, \ldots, N, \tag{9}$$

which specify that each of the fibres has no net force or torque acting on it, respectively, yields a coupled set of integral equations. These can be numerically solved for the velocity, angular velocity, and singularity distribution of each fibre.

Equations (7), (8), and (9) model interactions among N fibres in an unbound suspension. In order to model an infinite suspension, we use periodicity to replicate the N fibres in a unit cell throughout space. To determine the field disturbances created at any point in space due to a periodic distribution of Stokeslets we use the periodic solution of the Stokes flow equations, $\boldsymbol{H}_P(\boldsymbol{x})$, developed by Hasimoto (1959). This solution gives the disturbance velocity at a point due to a periodic distribution of identical Stokeslets *and* a net pressure gradient opposing the flow created by them. The latter is necessary to prevent divergence of the summation due to the slow (as

r^{-1}) decay of the disturbance created by individual Stokeslets. This is equivalent to the renormalization procedure discussed by O'Brien (1979) and Bonnecaze & Brady (1990). The periodic solution to the Stokes flow equations was evaluated using Ewald sums (Ewald 1921) to accelerate the convergence of the summations it contains.

Making use of $\boldsymbol{H}_P(\boldsymbol{x})$, the periodically extended version of (7) becomes

$$\begin{aligned}\boldsymbol{U}_j + \boldsymbol{\Omega}_j \times s\boldsymbol{p}_j = \boldsymbol{v}^{\infty}(\boldsymbol{x}_{cj} + s\boldsymbol{p}_j) + \sum_{\substack{i=1\\ i\neq j}}^{N} \int \boldsymbol{H}_P(\boldsymbol{x}_{c_i} + s'\boldsymbol{p}_i - \boldsymbol{x}_{c_j} - s\boldsymbol{p}_j) \cdot \boldsymbol{F}_i(s')\mathrm{d}s' \\ + \int \left[\boldsymbol{H}_P((s-s')\boldsymbol{p}_j) - \boldsymbol{H}((s-s')\boldsymbol{p}_j)\right] \cdot \boldsymbol{F}_j(s)ds \\ + 2\left(\ln 2A + \ln \frac{(1-s^2)^{1/2}}{\hat{b}(s)}\right)(\boldsymbol{\delta} + \boldsymbol{p}_j\boldsymbol{p}_j) \cdot \boldsymbol{F}_j(s) \\ + (\boldsymbol{\delta} - 3\boldsymbol{p}_j\boldsymbol{p}_j) \cdot \boldsymbol{F}_j(s) + (\boldsymbol{\delta} + \boldsymbol{p}_j\boldsymbol{p}_j) \cdot \int \frac{\boldsymbol{F}_j(s) - \boldsymbol{F}_j(s')}{|s-s'|} ds' \quad j = 1, \ldots, N. \end{aligned} \tag{10}$$

Equations (8), (9), and (10) were solved to find the fibre velocities, angular velocities, and stokeslet distributions, $\boldsymbol{F}_j(s)$. Using the latter, $\langle \boldsymbol{\sigma}^{(P)} \rangle$ can be determined from (4) and (1).

The above problem formulation considers all fibre–fibre interactions within the slender-body theory approximation. A wide variety of fibre shapes can be considered, since changing the fibre shape only changes the function $\hat{b}(s)$. Difficulties arise only for shapes such that $\mathrm{d}\hat{b}(s)/\mathrm{d}s > O(1)$, since our 'inner' solution in the method of matched asymptotic expansions (see Batchelor 1970) is not correct for such shapes. This difficulty is greatest when such relatively rapid variations in the body cross-section occur near the ends of fibre, since the errors involved in matching (5) to the "inner" solution become $O(1)$ or greater . For practical purposes, the only body shapes that cannot be simulated are blunt or nearly blunt-ended bodies. As will be shown in §5.2, the rheological properties of such suspensions are still well estimated by combining the results of simulations of non-blunt bodies and a simple analytical correction. Our Monte Carlo simulations can consider both linear and spatially periodic flow fields.

3. Numerical solution of the governing equations

In order to solve the governing equations, we first discretize the integrals using standard numerical integration techniques, i.e. $\int h(s)\mathrm{d}s \approx \sum_{k=1}^{k=M} w_k(s_k)h(s_k)$, where s_k are the discretization points and $w_k(s_k)$ are the weighting functions. Physical system parameters (the fibre shape, aspect ratio, orientation distribution, and volume fraction) and the unit cell parameters (its shape and the number of inclusions that it will contain) are specified and used to generate random, non-overlapping fibre positions and orientations. This reduces the discretized versions of equations (8), (9), and (10) to a set of $N \times (3M + 5)$ linear equations and unknowns. The unknowns for each fibre are three components of $\boldsymbol{F}(s)$ at each of the M discretization points, three components of $\boldsymbol{U}$, and two components of $\boldsymbol{\Omega}$. There are only two linearly independent components of angular velocity. This is because the slender-body theory approximation neglects variations in the velocity along a fibre cross-section. Thus, we can specify $\boldsymbol{\Omega} \cdot \boldsymbol{p} = 0$. The system of equations is solved by an LUD (Lower Upper Diagonal) matrix decomposition algorithm. We numerically integrate the resulting

stokeslet distributions to determine the fibre dipole tensors. These can be used with equations (1) and (3) to calculate the suspension stress. A typical simulation with $M = 13$ and 100 spheroidal inclusions in a cubic unit cell required about 5 minutes of CPU time on a CRAY C90 supercomputer. For each set of physical parameters, the equations were solved for 10–20 different particle configurations and the results were ensemble averaged.

Even after taking advantage of the fact that $\boldsymbol{H}_P(\boldsymbol{x}) = \boldsymbol{H}_P(-\boldsymbol{x})$, our simulations still required approximately $(N \times M)^2/2$ evaluations of $\boldsymbol{H}_P(\boldsymbol{x})$. These evaluations are computationally intensive, even though these are performed using Ewald sums, as discussed by Hasimoto (1959). We optimized this technique as a function of unit cell dimensions in order to minimize the number of calculations required to achieve a desired accuracy in $\boldsymbol{H}_P(\boldsymbol{x})$ using an algorithm developed by Mackaplow (1995) which chooses the adjustable parameter, α, and the various limits of summation in the Ewald sums, as a function of unit cell dimensions in order to minimize the number of terms required to get convergence. (See also *Note added in proof*, p. 185.)

In order to generate suspensions of fibres, a random number generator is first used to generate a fibre centre position within the unit cell, all positions being equally probable, and an orientation vector chosen from the appropriate distribution function. This fibre is placed in the unit cell. Then, the procedure is repeated, each time checking if the generated fibre position will overlap with a fibre that has already been placed in the unit cell or one of its periodic extensions. If it does, the proposed fibre is rejected. For isotropically oriented inclusions, since a fibre is less likely to overlap with a nearby fibre if the orientation vectors are similar (Doi & Edwards 1989), our procedure will lead to a certain degree of local orientation correlation within the unit cell. Since at the highest concentrations we study, the unit cells have dimensions less than 2 fibre lengths, there is a risk that this procedure will lead to a strongly preferred suspension orientations. To test for this, we divided the hemisphere of possible fibre orientations (taking advantage of the fore-aft symmetry of the fibres) into five equal-size regions. Then, histograms of the distributions were generated. We kept track of the maximum number of fibres in any one region. The average of this number was then calculated over the different configurations making up the ensemble average. This number, on average, was only 25% greater than the mean. More importantly, this percentage was constant over a wide range of suspension concentrations (and thus unit cell sizes). Thus, we conclude that our suspension generation method did not strongly bias the orientation distribution in our model suspensions. The procedure to generate model suspensions with the orientation distribution found in steady-state shear flow is somewhat more complicated and will be discussed in §5.

Our method of generating model suspensions does not lead to configurations in which all non-overlapping configurations are equally probable. Such a distribution would be the equilibrium configuration for a Brownian suspension. However, for our non-Brownian system, it is not clear if this is ever a relevant distribution.

Nevertheless, we must question how much our results are dependent on the local fibre orientation correlations and centre-of-mass distributions produced by our particular generation algorithm. Insight into this can be gained by considering the corrections to the dilute theory for two-body interactions and the semi-dilute theories of Shaqfeh & Fredrickson (1990). These theories explicitly consider particle interactions. They also ignore excluded volume effects. Thus, their predictions are based on no orientation correlations between particles. We note that it is the fibres closest to a given 'test fibre' that will have the greatest effect on its stresslet. The above theories predict the effect of particle interactions on the mean particle stresslet

to be nearly independent of particle orientation distribution. Thus, we believe that the effect of fibre interactions on the mean particle stresslet is independent of any local orientation correlations. We also see good agreement between the results of our simulations, the semi-dilute theory, and experimental data. Since all three systems produce particle configurations in different ways, they presumably have slightly different centre-of-mass distributions. Thus, the good agreement between the three sets of data suggests that our results are independent of the details of the centre-of-mass distribution.

Based on the above, over the concentration range investigated, we believe our simulation results are independent of the details of the suspension generation algorithm. Only algorithms that produce grossly inhomogeneous distributions, or, in the case of attempting to produce isotropic distributions, macroscopically anisotropic distributions, should be considered suspect.

When generating model suspensions of aligned fibres, overlap between any two fibres is tested by using straightforward geometrical considerations. For isotropic inclusions, we can characterize any point t on the surface of a fibre as a point in a local polar coordinate system, $(\theta(t), \phi(t), \rho(\theta(t), \phi(t))$. The coordinate system is defined such that the origin is at the centre of the fibre and the ends of the fibre correspond to $\phi = 0$ and $\phi = \pi$. We can write this equation for any point q on another inclusion as well. Let us denote these two inclusions as I and II. These two points can both be converted to points in their respective local Cartesian coordinate systems, and using a coordinate transformation, we can find the distance between them. Finally, we use an unconstrained optimization algorithim (*Amoeba*, from Press *et al.* 1990) on the variables $\theta_I, \phi_I, \theta_{II}, \phi_{II}$ to minimize this distance. If the minimum distance is zero, within our total roundoff error, we say that the two fibres overlap.

Many different numerical integration algorithms were tested to solve the integral equations. Gauss–Legendre Quadrature was used predominately in the simulations since it generally converged with the least computational effort. Our simulations typically required 13 discretization points/ integral to get numerical convergence within 1% for non-dilute suspensions. This value of 13 was determined from studies in which the mean dipole of a given fibre configuration was monitored as the number of discretization points was varied from 7 to 25.

Concerning the use of periodicity, we require that the unit cell size be sufficiently large that our results are not altered by fibres interacting with their own periodic extensions. We tested for these 'box size' effects by holding all of the physical system parameters constant (suspension volume fraction, particle geometry, etc.) but varying the size and shape of the unit cell, as well as the number of particles it contained. We then observed how this affected the ensemble-average particle dipole tensor. These results allowed us to choose the size and shape of our unit cell for our simulations such that they always have less than a 1% effect on the average dipole tensor. All of our unit cells are longitudinally rectangular with square cross-sections. This shape makes it easier to both optimize Ewald's technique (Mackaplow 1995) and physically visualize geometric relationships between fibres in neighbouring unit cells. For the simulations of suspensions of aligned fibres, rectangular unit cells were used which were 6 times longer in the direction of fibre alignment than perpendicular to it. For simulations where the fibres were not perfectly aligned (e.g. isotropic suspensions), cubic unit cells were used. The number of fibres per unit cell varied from 50 to 175. Typically, 100 fibres per unit cell proved to be the best balance between minimizing computational effort per configuration and maximizing unit cell size.

4. Theoretical predictions

The most general form of $\langle \boldsymbol{\sigma}^{(P)} \rangle$ for an unbound fibre suspension can be written (Batchelor 1971)

$$\langle \boldsymbol{\sigma}^{(P)} \rangle = \left[\mu^{FIBRE} \left(\langle \boldsymbol{pppp} \rangle - \boldsymbol{\delta} \langle \boldsymbol{pp} \rangle /3 \right) : \langle \mathbf{e} \rangle \right] \times \left(1 + O(A^{-2} \ln(A)) \right). \tag{11}$$

μ^{FIBRE} is a dimensional constant that is a function of the physical parameters in the suspension. The error term results from neglecting the effect of gradients in the undisturbed flow field along the fibre cross-sections. To present theoretical predictions and our numerical results we will use a factor called Q, defined

$$Q \equiv \frac{3}{8\pi n l^3} \left(\frac{\mu^{FIBRE}}{\mu} \right). \tag{12}$$

As we shall show, examining Q facilitates determining the screening behaviour of the suspension. Analysis of the equivalent versions of Q for heat and mass transfer through fibre suspensions were successfully used in our previous study (Mackaplow *et al.* 1994) to determine suspension screening lengths. Using (4), (11), and (12) we can relate Q to moments of the fibre orientation distribution function, the externally imposed flow field, and the numerically determined average particle stresslet:

$$Q \times \left[\langle \boldsymbol{pppp} \rangle - \boldsymbol{\delta} \langle \boldsymbol{pp} \rangle /3 \right] : \langle \mathbf{e} \rangle \equiv 3 \langle \mathbf{S} \rangle \tag{13}$$

where we have used the non-dimensionalizations discussed in the previous section. It is valid to use a single scalar constant, Q, to relate $\langle \mathbf{S} \rangle$ and $\left[\langle \boldsymbol{pppp} \rangle - \boldsymbol{\delta} \langle \boldsymbol{pp} \rangle /3 \right] : \langle \mathbf{e} \rangle$ since over the ensemble average, both of these tensors will have the same tensorial form. We have verified this from our simulations.

4.1. *Dilute suspensions*

For dilute suspensions, μ^{FIBRE} (and therefore Q) is not a function of the particle orientation distribution, thus the entire effect of the particle orientation distribution on $\langle \boldsymbol{\sigma}^{(P)} \rangle$ is explicitly accounted for by the factor of $\langle \boldsymbol{pppp} \rangle - \boldsymbol{\delta} \langle \boldsymbol{pp} \rangle /3$. In such cases, the theoretical analysis of Batchelor (1970) based on slender-body theory can be used to show that

$$Q^{Dilute} = \frac{1}{2\left[\ln(2A) + g(A)\right]} \tag{14}$$

where $g(A)$ depends on the fibre shape. In particular, for spheroids he showed

$$Q^{Dilute}_{spheroids} = \frac{1}{2\left[\ln(2A) - 1.5\right]} \tag{15}$$

and for cylinders

$$Q^{Dilute}_{cylinder} = \frac{1}{2\ln 2A} \left[\frac{\ln 2A + 0.640}{\ln 2A - 1.5} + \frac{1.659}{(\ln 2A)^2} + O\left(\frac{1}{\ln 2A} \right)^3 \right]. \tag{16}$$

4.2. *Corrections at* $O(nl^3)$

A dilute theory for aligned suspensions that takes into account two-body interactions is developed in the Appendix

$$Q^{2-body}_{Aligned} = Q^{Dilute} + \frac{0.206 n l^3}{\ln^3(2A)}. \tag{17}$$

The analogous theory for isotropic suspensions was developed by Shaqfeh & Fredrickson (1990). However, due to an algebraic error, the coefficient multiplying the correction term was in error. The corrected theory is

$$Q_{Isotropic}^{2-body} = Q^{Dilute} + \frac{0.222nl^3}{\ln^3(2A)}. \tag{18}$$

This correction has not been previously presented and is also developed in the Appendix. Within the accuracy of the theoretical analysis, these correction terms are independent of fibre shape.

4.3. *Semi-dilute theories*

If the disturbance velocity created by a fibre in a suspension decays more rapidly than it would if no other fibres were present, screening is said to occur. This is discussed in more detail by Shaqfeh & Fredrickson (1990). According to cell models

$$Q = \frac{1}{2\ln(\chi/b)} \tag{19}$$

where χ is the 'screening length', i.e. the average distance over which the velocity disturbance propagates. Two important geometric length scales in semi-dilute suspensions are the *average interfibre spacing*, h_{av}, the average distance that one must move perpendicularly from any point on the axis of a fibre before intersecting another fibre, and the *average closest approach distance*, h_{ca}, between a fibre and its nearest neighbor. For aligned suspensions, both h_{av} and h_{ca} have the same scaling with fibre volume fraction ϕ. In the semi-dilute regime

$$\frac{h_{av}}{b}|_{aligned,isotropic} \sim O\left(\frac{1}{\phi}\right)^{1/2}.$$

Batchelor (1971) proposed that this would be the suspension screening length, leading to

$$Q|_{aligned}^{Batchelor} = \frac{1}{\ln(1/\phi) + C} \tag{20}$$

where C is an unknown $O(1)$ constant.

For isotropic suspensions, although h_{av} scales in the same way as for aligned suspensions, h_{ca} scales very differently (Doi & Edwards 1989):

$$\frac{h_{ca}}{b}|_{isotropic} \sim O\left(\frac{A}{nl^3}\right)$$

where we again note that n is the number density of fibres and l is the fibre half-length. In the semi-dilute regime $h_{ca} \ll h_{av}$. Dinh & Armstrong (1984) proposed that the screening length would be approximately h_{ca}, leading to the same prediction for aligned suspensions, (20), but a very different one for isotropic suspensions

$$Q|_{isotropic}^{D\&A} = \frac{1}{\ln(A/nl^3) + C'}. \tag{21}$$

Unlike previous investigators, who simply assumed a suspension screening length, Shaqfeh & Fredrickson (1990) used slender-body theory and a multiple scattering analysis, to find

$$Q|^{S\&F} = \frac{1}{\ln(1/\phi) + \ln\ln(1/\phi) + C'' + O\left((1/\ln\phi)\right)} \tag{22}$$

where each term in the series represents the effect of a certain class of fibre–fibre interactions. C'' is an $O(1)$ constant that is a function of fibre shape and orientation distribution. Comparing (22) to (19) yields $\chi/b \sim [(1/\phi)\ln(1/\phi)]^{1/2}$ for all orientation distributions, assuming randomness in the centre-of-mass. By neglecting the $[\ln(1/\phi)]^{1/2}$ part of this expression, we see that this analysis predicts that the screening length is approximately equal to the average interfibre spacing. This is in contrast to the prediction of Dinh & Armstrong (1984).

As discussed by Mackaplow *et al.* (1994), some of the values of C'' shown in Shaqfeh & Fredrickson(1990) are incorrect. This results from Shaqfeh & Fredrickson (1990) assuming that the suspension volume fraction, ϕ, is $2\pi nl^3/A^2$, regardless of fibre shape, even though this is only true for cylinders. The corrected values for spheroidal fibres are 1.034 and 0.202 for aligned and isotropic suspensions, respectively. The corresponding values for cylindrical fibres are 0.1585 and −0.6634.

5. Results and discussion

5.1. *Determination of suspension screening behavior*

In our initial simulations we systematically varied nl^3 by changing either the fibre aspect ratio *or* the suspension volume fraction. This was done in order to verify the accuracy of our simulations, compare them to existing theories, and determine screening behaviour. All of the simulations were performed using spheroidal fibres in an externally imposed planar extensional flow, i.e.

$$\boldsymbol{v}^{\infty}(\boldsymbol{x}) = \dot{\gamma} \begin{vmatrix} 1 & 0 & 0 \\ 0 & -1 & 0 \\ 0 & 0 & 0 \end{vmatrix} \cdot \boldsymbol{x}.$$

In our analogous numerical study of heat and mass transport through fibre suspensions (Mackaplow *et al.* 1994), we directly simulated both spheroidal and cylindrical fibres. We found no qualitative difference in the suspension screening lengths between suspensions of spheroids and cylinders. Based on the similarity of the governing equations for those two physical systems to those of the system considered here, we expect that suspensions of cylinders will have the same qualitative hydrodynamic screening behaviour as suspensions of spheroids. Additionally, Q and μ_{FIBRE} will be independent of our choice of flow field.

5.1.1. *Aligned suspensions*

Figures 1(*a*) and 1(*b*) show plots of Q *vs.* nl^3 for fibres with an aspect ratio of 100 that are all aligned with the principal axis of extension of the imposed flow field. For each set of simulations we have shown the mean and its 95% confidence interval.

In figure 1(*a*) we see that for $nl^3 \ll 1$, Q is constant. This means that the contribution of the particles to the stress in the suspension is directly proportional to the volume fraction of fibres. These results are in excellent qualitative and quantitative agreement with the dilute theory of Batchelor (1970). For $nl^3 \geqslant O(1)$, we see a positive deviation from the dilute theory, showing that fibre–fibre interactions are further enhancing the particle stress beyond the dilute theory prediction. This is in qualitative agreement with the version of the dilute theory that is corrected to take into account two-body interactions, developed in the Appendix. The semi-dilute theory of Shaqfeh & Fredrickson (1990) is qualitatively similar to our simulation data for $nl^3 \gg 1$, but quantitatively lies 25%–30% below it. However, by adjusting the constant, C'',

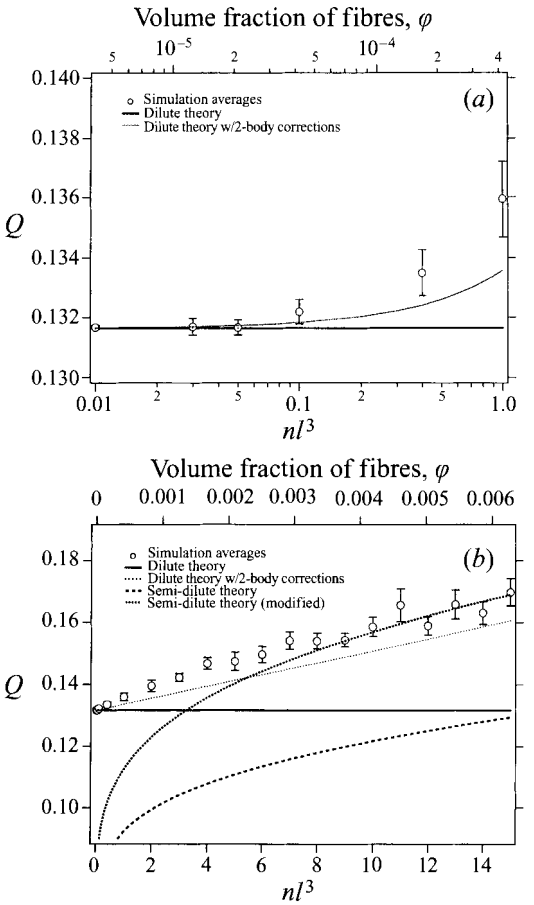

FIGURE 1. Normalized extra particle stress, Q, of a suspension of aligned, spheroidal fibres with aspect ratio, $A = 100$, as a function of the suspension volume fraction. Shown are the predictions of numerical simulations, the dilute theory (with and without two-body corrections), and the semidilute theory of Shaqfeh & Fredrickson (1990) (both the original and modified versions).

in the semi-dilute theory from the value given by Shaqfeh & Fredrickson (1990), 1.034, to -1.25, and assigning a coefficient of 2.4 to the $O(1/\ln(1/\phi))$ term, a much better quantitative agreement with the simulations is achieved. This is shown in figure 1(*b*). As will be subsequently shown in figures 2, 3, and 4, by utilizing these particular adjusted coefficients the semi-dilute theory is in an excellent quantitative agreement with the simulations for suspensions having a wide range of concentrations and particle aspect ratios. The need to adjust C'' and keep the $O(1/\ln(1/\phi))$ term corresponds to keeping classes of interparticle interactions that are neglected in the asymptotic theory. Thus, it appears the scaling predicted by Shaqfeh & Fredrickson (1990) is correct, but more terms in the series must be kept to get good quantitative accuracy.

Of particular interest is the fact that the dilute theory with two-body corrections predicts, with small error, the behaviour of the suspension at concentrations up to $nl^3 = 15$. This is interesting because this theory was developed to be valid only in the dilute region. One indicator of the breakdown of the two-body theory is when the correcting term to the dilute theory become of the same order as the term it is correcting. This does not occur until $nl^3 \sim O(\ln^2(2A))$. For an aspect ratio of 100,

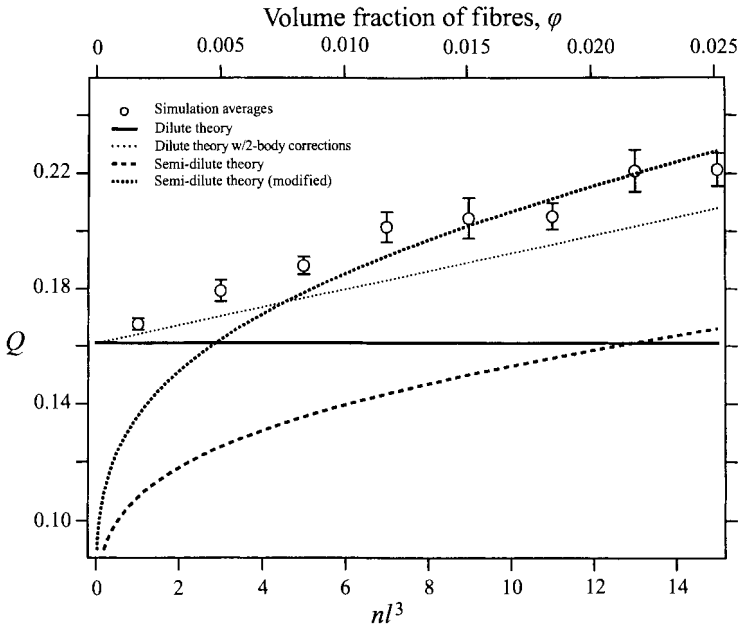

FIGURE 2. Normalized extra particle stress, Q, of a suspension of aligned, spheroidal fibres with aspect ratio, $A = 50$, as a function of the suspension volume fraction. Shown are the predictions of numerical simulations, the dilute theory (with and without two-body corrections), and the semi-dilute theory of Shaqfeh & Fredrickson (1990) (both the original and modified versions).

$\ln^2(2A) \approx 30$. The ability of dilute theories that incorporate the effects of two-body interactions to predict suspension behaviour into the semi-dilute concentration regime was also observed in our previous study of heat transfer through suspensions of highly conducting fibres (Mackaplow *et al.* 1994).

Figure 2 shows a plot of Q *vs.* nl^3 for suspensions of fibres with an aspect ratio of 50. All of the fibres are aligned with the principal axis of extension of the flow field. As in figure 1(*b*), we see that by using the adjusted coefficients in the semi-dilute theory of Shaqfeh & Fredrickson (1990), an excellent agreement between simulations and theory can be achieved for $nl^3 \gg 1$.

Figure 3 shows a plot of Q *vs.* nl^3 for suspensions with a fixed inclusion volume fraction, ϕ, of 6.67×10^{-5} . Again, there is a positive deviation from dilute theory for $nl^3 \geqslant O(1)$. Note that Q approaches a constant in the semi-dilute regime. This is consistent with the prediction of the semi-dilute theory that the non-dimensionalized screening length in a semi-dilute suspension, χ/b, is only a function of the volume fraction of the suspension. Whereas the published semi-dilute theory of Shaqfeh & Fredrickson (1990) quantitatively underestimates this value by approximately 20%, by utilizing the adjusted coefficients, excellent quantitative agreement is achieved. As for the previous sets of simulations, the dilute theory with two-body corrections does a good job of predicting the suspension rheology over the entire range of concentrations studied.

In our previous study of heat and mass transfer through fibre suspensions, similar scalings of the suspension screening length in the semi-dilute regime were observed, as predicted by the theory of Fredrickson & Shaqfeh (1989). However, in this previous study we found that using the theoretically predicted value of C'' and neglecting the

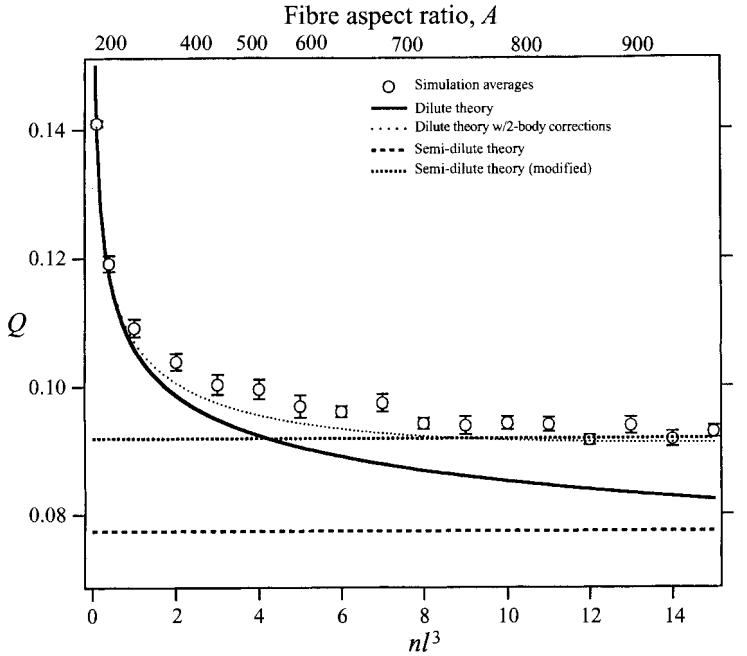

FIGURE 3. Normalized extra particle stress, Q, of a suspension of aligned, spheroidal fibres with a volume fraction of $\phi = 6.67 \times 10^{-5}$, as a function of fibre aspect ratio. Shown are the predictions of numerical simulations, the dilute theory (with and without two-body corrections), and the semi-dilute theory of Shaqfeh & Fredrickson (1990) (both the original and modified versions).

$O(1/\ln(1/\phi))$ term resulted in much better agreement with the simulation data than in the present study. The reason for this discrepancy is still unknown.

5.1.2. *Isotropic suspensions*

Figure 4 shows the results for isotropic suspensions with a fixed inclusion volume fraction of 6.67×10^{-5}. Note that the error bars are much larger than for the aligned simulation data. This is because whereas for an aligned suspension a group of non-interacting particles will all have the same dipole tensor, for an isotropic suspension a particle's dipole tensor strongly depends on its orientation with respect to the imposed external flow field. Thus, the slight differences in moments of the fibre orientation distributions between different suspension realizations contributes to the variance in the ensemble average.

For $nl^3 < 1$ we see good agreement with the dilute theory. At concentrations greater than this, the simulations show a positive deviation from the dilute theory. Q approaches a constant in a manner very similar to the simulations of aligned suspensions shown in figure 3. This agrees qualitatively with the theoretical predictions of Shaqfeh & Fredrickson, which quantitatively lie 10%–15% below the simulation data. However, the simulation data are in qualitative and quantitative disagreement with the theoretical prediction of Dinh & Armstrong (1984) based on fibre disturbances being screened on the same length scales as the closest approach distances between fibres. This theory, which predicts Q to increase monotonically with increasing nl^3, greatly overestimates Q.

As in the case of aligned fibre suspensions, using the adjusted coefficients in the semi-dilute theory of Shaqfeh & Fredrickson results in excellent quantitative

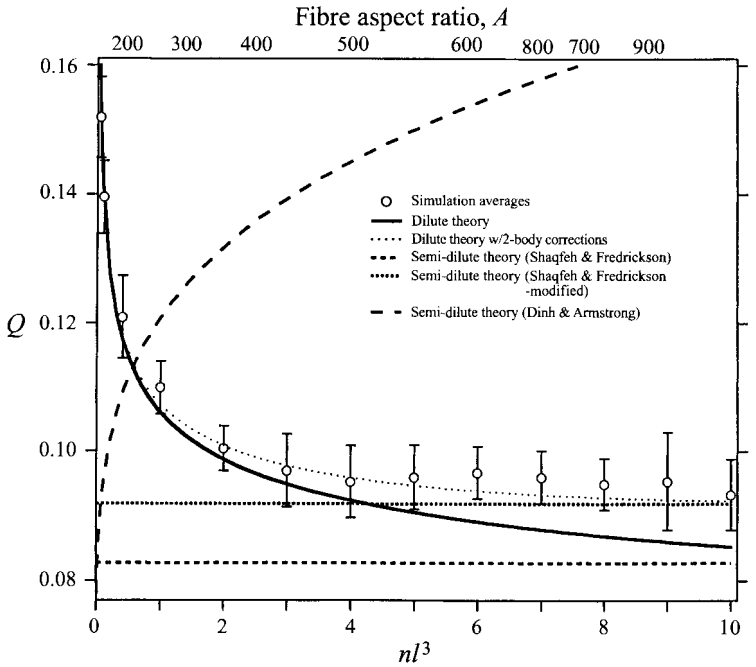

FIGURE 4. Normalized extra particle stress, Q, of a suspension of isotropic, spheroidal fibres with a volume fraction of $\phi = 6.67 \times 10^{-5}$, as a function of fibre aspect ratio. Shown are the predictions of numerical simulations, the dilute theory (with and without 2-body corrections), and the semi-dilute theories of both Dinh & Armstrong (1984) and Shaqfeh & Fredrickson (1990) (both the original and modified versions).

agreement between the theory and simulations in the semi-dilute concentration regime. The dilute theory that takes into account two-body interactions does a very good job of predicting the suspension rheology over the entire range of concentrations studied.

5.1.3. *Comparison of aligned and isotropic suspensions*

In order to compare the screening behaviour in aligned and isotropic suspensions more quantitatively, in figure 5 we have plotted the simulation results from figures 3 and 4 on a common set of axes. We see very good agreement between the two sets of data. Using (19), this shows that the suspension screening lengths for these two very different fibre orientation distributions, aligned and isotropic, are approximately the same not only in the dilute regime, but at all concentrations up through semi-dilute.

It is of interest to compare the screening length in a semi-dilute suspension of force-free fibres to that in a fibrous porous medium. These physical systems are very different. This is particularly so on length scales of the order of a fibre length. In one system the fibres are force-free and in the other they are not. However, Shaqfeh & Fredrickson (1990) predicted that on much smaller length scales the propagation of velocity disturbance will be screened in the same way in both systems. On these length scales, a disturbances will be mainly effected by the parts of the fibres closest to it. Thus, it might not experience the fibres as force-free objects, but objects with a net forces associated with them. This, of course, will not hold on length scales of the fibre length or longer.

By finding the Green's function for the Brinkman (1947) equation, Howells (1974) showed that the screening length in a porous medium is the square root of its permeability. Surveys of experimental and theoretical studies of the permeability of fibrous

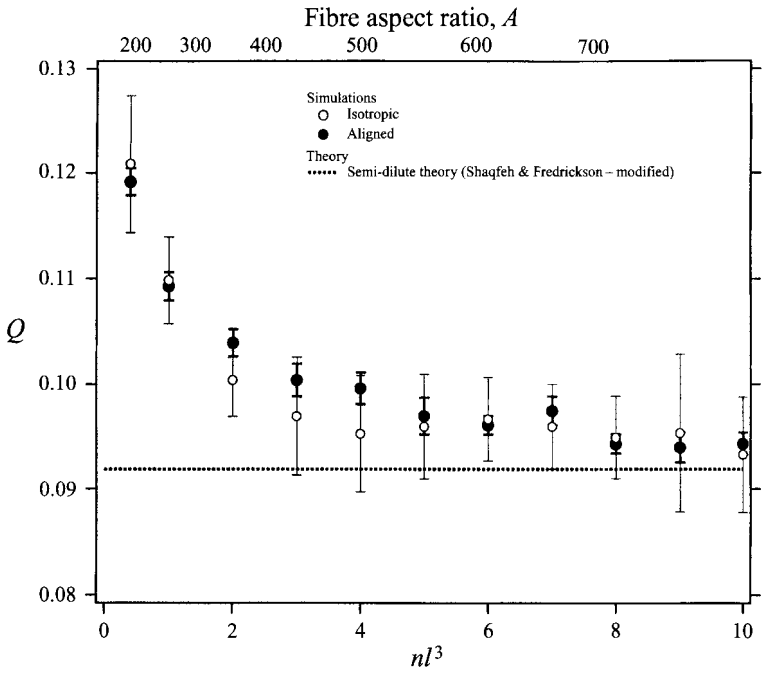

FIGURE 5. Comparison of normalized extra particle stress, Q, of aligned and isotropic suspensions of spheroidal fibres with a volume fraction of 6.67×10^{-5}, as a function of fibre aspect ratio. Also shown is the modified version of the semidilute theory of Shaqfeh & Fredrickson (1990).

porous media are presented by Koch & Brady (1986) and Jackson & James (1986). The results predict that in the limit of small volume fraction, the screening length in fibrous porous media, χ_{PM}, is given by

$$\frac{\chi_{PM}}{b} = \left(\frac{C^{PM}}{\phi} \ln \frac{1}{\phi}\right)^{1/2}. \tag{23}$$

b is the characteristic fibre width. C^{PM} equals 1/8, 1/4, and 3/20 for flow perpendicular to aligned fibres, parallel to aligned fibres, and through isotropically oriented fibres, respectively. The semi-dilute theory of Shaqfeh & Fredrickson (1990) for the rheology of fibre suspensions, (22), predicts

$$\frac{\chi}{b} = \left(\frac{e^{C''+B/\ln(1/\phi)}}{\phi} \ln \frac{1}{\phi}\right)^{1/2}. \tag{24}$$

Using the values of C'' determined by our best fit to simulation data, -1.25, results in $e^{C''+B(1/\ln(1/\phi))} \approx 0.3$ in the low volume fraction limit for both isotropic and aligned configurations. Thus our measured screening length in semi-dilute suspensions of force-free fibres is qualitatively and quantitatively very similar to those in fibrous porous media. This is consistent with the analysis of Shaqfeh & Fredrickson (1990). This is similar to the conclusion reached in our numerical study of heat and mass transport in fibre suspensions (Mackaplow *et al.* 1994). In that study it was shown that the screening length for heat transport through suspensions of highly conducting fibres, where no fibre is a net source nor sink of heat, is the same as that in the classical reaction-diffusion problem with fibres, where each fibre is a net sink of reactant.

5.1.4. *Decay of point singularities*

In our simulations of suspension rheology, we tested for screening by studying the scaling of the fibre stress with fibre concentration and aspect ratio. We can also test for screening by studying the decay of the velocity field created by point singularities. The velocity induced by an isolated point force in a fibre-free fluid decays as $1/r$, where r is the distance from the point force. If the velocity is screened on a length scale χ, it will decay approximately as

$$v \sim \mathrm{e}^{-r/\chi}/r \tag{25}$$

over length scales of $\leqslant O(\chi)$.

One possible way to test for screening is to allow the undisturbed velocity field in a fibre suspension be that created by a periodic distribution of stokeslets. We could then analyse the velocity in the direction of the stokeslets, v_s, as a function of radial distance from the closest stokeslet. In this system, the adverse pressure gradient necessary for renormalization drives a flow in the *opposite* direction to the stokeslets in approximately half of the fluid. It follows, that even in the absence of particles, the velocity field will decay on length scales of approximately $H/4$, where H is the characteristic box length. Thus, in order to distinguish any suspension screening from the natural decay of the singularities, we would require $H/4 \gg \chi$. Unfortunately, since our computational effort $\sim H^9$, for semi-dilute suspensions the largest we can make our periodic boxes is $H \approx 8\chi$, which is too small to distinguish suspension screening.

At this point, one might wonder if our periodic boxes introduce an artificial screening into our simulations of suspension rheology. They do not. This is because the aforementioned artificial screening is due entirely to the net adverse pressure gradient required to renormalize the forcing stokeslets. In our simulations of suspension rheology, since the fibres are force free, there is no net adverse pressure gradient for renormalization. Thus, there is no artificial screening.

Durlofsky & Brady (1987) studied the propagation of velocity disturbances in porous media by placing forcing functions at the centre of the unit cells. They compared the propagation of the velocity disturbance in both finite and periodically extended systems and found little difference at points within the unit cell. This suggests that we might be able to observe screening using a non-periodically extended system. To test this, we generated a finite suspension by placing 150 spheroidal fibres, aspect ratio = 663, such that all of the fibre centres were in a cubic unit cell. To not bias the distribution relative to an unbound suspension, fibre positions were rejected if they overlapped with any other fibres in the box *or* any of their periodic extensions (if they were to exist). The cell size, $H \approx 2.8l$, corresponded to a suspension concentration of $nl^3 = 7$. Equation (24) predicts $\chi \approx 0.35l$.

Simulations identical to those discussed earlier were performed, except that the undisturbed velocity field was given by a stokeslet placed at the centre of the unit cell. The locations of 30 equally spaced concentric circles with radii ranging from $\chi/15$ to 2χ, in the plane perpendicular to the point force, were calculated. Along each of these circles, the velocity was calculated at 8 equiangularly-spaced points. This was usually done using

$$\boldsymbol{v}(\boldsymbol{x}_G) = \boldsymbol{H}(\boldsymbol{x}_G - \boldsymbol{x}_M) \cdot \boldsymbol{F}_S + \sum_{i=1}^{N} \int \boldsymbol{F}_i(s) \cdot \boldsymbol{H}(\boldsymbol{x}_G - \boldsymbol{x}_{c,i} - s\boldsymbol{p}_i)\mathrm{d}s \tag{26}$$

where $\boldsymbol{H}(\boldsymbol{x})$ is the Oseen tensor, and $\boldsymbol{x}_M$ is the centre of the unit cell. $\boldsymbol{x}_G$ may be any one of the 240 points at which we calculate the velocity, and the axial stokeslet

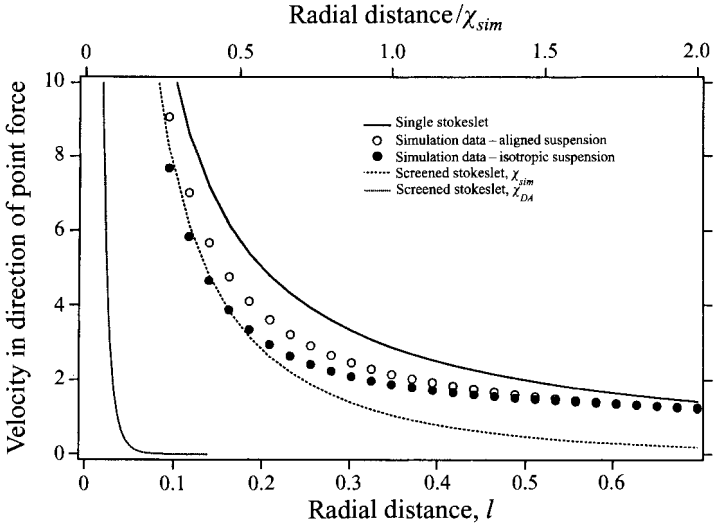

FIGURE 6. Decay of the velocity, v_z, created by a point force in a unit cell as a function of radial distance, r, in the plane perpendicular to the point force. The simulation results for unit cells containing both aligned and isotropic fibre suspensions are shown. The unit cell contains 150 spheroids having an aspect ratio of 663, for an effective concentration of $nl^3 = 7$. Also shown are the decay of an isolated stokeslet, and stokeslets screened on length scales of χ_{sim} and χ_{DA}.

distributions $\boldsymbol{F}_i(s)$ were calculated from the simulation. $\boldsymbol{F}_s$ is the forcing stokeslet. We have taken the centre of the unit cell to be the origin. Approximately 1 out of every 400 values of $\boldsymbol{x}_G$ lay within $5b$ of a fibre axis. At these points the velocity was approximated as the fibre velocity at the closest axial position. Both aligned fibres (aligned in the direction of the stokeslet) and isotropic fibre orientation distributions were considered. For each orientation distribution, the results were ensemble averaged over 10 different particle realizations.

Figure 6 shows the mean suspension velocity in the direction of the stokeslet, $\langle v_z \rangle$, as a function of radial distance away from the stokeslet, r. Also shown are the velocity profiles of an unscreened stokeslet, and stokeslets screened at both the length scales predicted by our simulations of rheological properties, χ_{sim}, and that predicted by Dinh & Armstrong for an isotropic suspension, χ_{DA}. We see that the velocity field in the fibre suspension decays much more rapidly than that of an isolated stokeslet. The length scale of this screening is approximately χ_{sim} in both aligned and isotropic suspensions. Although the decay of the velocity field is slightly faster in the isotropic suspensions, it is not nearly as fast as predicted by Dinh & Armstrong (1984). The screening behaviour is more evident in figure 7, where we have $v_z(r) \times r$ as a function of r.

In figures 6 and 7 we observe a slower decay of the velocity field at radial distances greater than approximately $\chi_{sim}/2$. This contrasts with the continued exponential decay predicted by equation (25). This is because for length scales $\geqslant O(\chi)$, equation (25) only holds for a fixed porous medium. In such, the inclusions exert a net force and damp the imposed velocity field at all length scales. In contrast, in a suspension of force-free inclusions, the inclusions serve to transfer momentum over the length scale of the inclusions and eventually the medium appears to be a viscous fluid. Thus after the initial rapid decline, the velocity field decays slower than $1/r$ over length scales of $O(l)$.

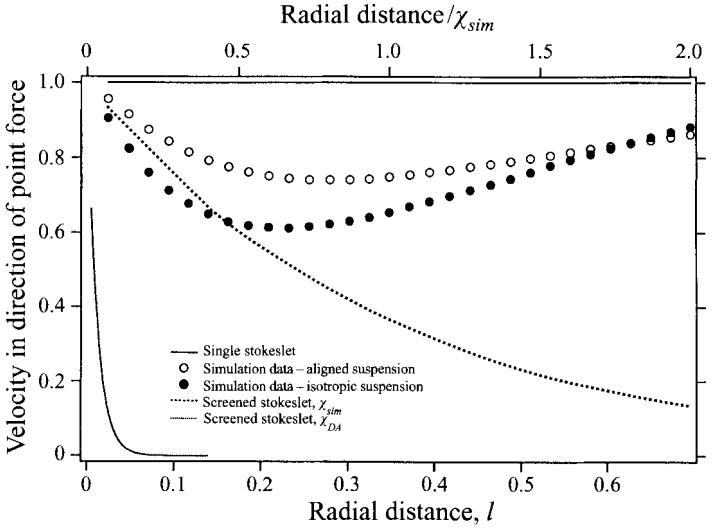

FIGURE 7. Decay of the velocity field *multiplied by radial distance*, $r \times v_z$, created by a point force in a unit cell as a function of radial distance, r, in the plane perpendicular to the point force. The simulation results for unit cells containing both aligned and isotropic fibre suspensions are shown. The unit cell contains 150 spheroids having an aspect ratio of 663, for an effective concentration of $nl^3 = 7$. Also shown are the decay of an isolated stokeslet, and stokeslets screened on length scales of χ_{sim} and χ_{DA}.

5.2. *Comparison of simulation results to experimental data*

We will now compare our simulations to published experimental data. However, all these studies involved suspensions of cylindrical fibres. We could not directly simulate suspensions of cylinders. Instead, we simulated suspensions of spheroids having the same aspect ratios and nl^3 value as the suspensions used in the experiments. These simulation results were then scaled using the ratio of the dilute theoretical prediction for cylinders (equation (16)), to that for spheroids (equation (15)). This physically corresponds to an isolated cylinder having the same particle stresslet as a spheroid with a larger aspect ratio, A_{eff}, where $A_{eff} > A$. However, the percentage enhancement of the stresslet due to interparticle interactions will still depend only on nl^3. We have based this conversion method on the findings of our analogous study of heat and mass transport through fibre suspensions (Mackaplow *et al.* 1994), where converged numerical results were obtained for both spheroidal and cylindrical fibres.

We have not attempted comparisons to falling-ball rheometry studies, such as those by Milliken *et al.* (1989). Such investigations determine the 'effective viscosity' of fibre suspensions by measuring the fall speed of a sphere sedimenting through the suspension. The flow field created by a sedimenting sphere will induce a local fibre ordering that decays away from the sphere. Since it is the fibres closest to the sphere that will have the greatest effect on its fall velocity, comparisons of these results to our simulations of isotropic suspensions are not meaningful. Additionally, the numerical simulations of falling-ball rheometry by Harlen, Sundarajakumar & Koch (1995) show that even in the dilute regime, fibre contacts, which we neglect, substantially increases the 'effective viscosity'. We note this was not found to be the case in sheared suspensions.

Investigators	A	ϕ (%)	nl^3	Dilute theory	Semi-dilute theory	Experiments	Simulations
P & B (1990)	50	0.14	0.56	1.3	1.2	1.3	1.3
	50	0.30	1.2	1.6	1.5	1.5	1.8
	50	0.90	3.6	2.9	2.7	3.4	3.3
W (1970)	57	1.3	6.7	4.4	4.1	9	5.1
M & M (1974)	282	0.930	118	40	53	52	60
	586	0.099	54	16	18	19	20
	586	0.287	157	45	57	75	65
	1259	0.096	242	60	76	60	88

TABLE 1. Extensional viscosity of suspensions of cylindrical fibres extruded through a circular, horizontal orifice, relative to that for the fibre-free liquid. Shown are the experimentally determined values for the investigations listed (Pittman & Bayram 1990; Weinberger 1970; Mewis & Metzner 1974), as well as the predictions of numerical simulations, the dilute theory, and the semidilute theory of Shaqfeh & Fredrickson (1990).

5.2.1. *Aligned fibres in a uniaxial extensional flow*

Weinberger (1970), Mewis & Metzner (1974), and Pittman & Bayram (1990), among others, have studied the rheology of jets of suspended fibres extruded in the direction of gravity from a horizontal, circular orifice. The particle-free flow in such jets is approximately a uniaxial extensional flow with a rate of strain tensor given by

$$\mathbf{e}(\boldsymbol{x}) = \dot{\gamma}(\boldsymbol{x}\cdot\mathbf{1}) \begin{vmatrix} 1 & 0 & 0 \\ 0 & -\frac{1}{2} & 0 \\ 0 & 0 & -\frac{1}{2} \end{vmatrix},$$

where $\mathbf{1}$ is the direction of gravity and $\dot{\gamma}(x)$ is a decreasing function of x. In the absence of fibre–fibre interactions, all of the fibres in the suspension will align in the direction of gravity. It has been shown experimentally (Harris & Pittman 1976) and theoretically (Shaqfeh & Koch 1990; Sandstrom & Tucker 1993) that the effect of fibre interactions in extensional flows in the semi-dilute regime is to introduce some dispersion in the orientation distribution about the preferred direction, but the overwhelming majority of the fibres, particularly through semi-dilute concentrations, will be aligned with gravity. All of the investigators measure $\left(\sigma_{11}(z) - \frac{1}{2}\left(\sigma_{22}(z) + \sigma_{33}(z)\right)\right)/\dot{\gamma}(z)$ in the suspensions, whose value is independent of axial position. For a Newtonian fluid this ratio is 3μ, and is often referred to as the 'Trouton' or 'extensional' viscosity.

In table 1 we have compared the experimentally measured extensional viscosity relative to the Trouton viscosity for various suspensions to the predictions of the dilute theory, the semi-dilute theory of Shaqfeh & Fredrickson (1990), and the results of our simulations based on perfectly aligned fibres. In general, the qualitative and quantitative agreement between the experiments and simulations is good. Moreover, the overall agreement between the semi-dilute theory and the experimental data is similar to that between the simulations and the experimental data.

The major cause of the discrepancy between experiments and simulations is most likely the observed *jet instabilities*. These are large-amplitude, oscillatory variations in the radius of the jet as a function of axial position, which occur with greater severity with increasing fibre aspect ratio and suspension volume fraction, as noted by Mewis & Metzner (1974) and Pittman & Bayram (1990). Since experimental observables are related to the suspension stress using a momentum balance based on a smooth jet profile, such instabilities greatly reduce the experimental accuracy. Since Pittman &

Bayram (1990) noted the severity of the instability for each experiment performed, we have only compared our simulations to their experiments for *regular* jets. This probably accounts for the generally better agreement between their experimental data and our simulations as compared to the experimental data from other investigators. Other probable sources of the discrepancy between experiment and simulations are: (i) incomplete alignment and dispersion of fibres, (ii) jamming of the extrusion orifice by fibres, (iii) polydispersity of fibre aspect ratios, and (iv) the jet diameter being of the same order as the average interfibre spacing. These are discussed in more detail by Pittman & Bayram (1990).

5.2.2. *Isotropic fibres in shear flow*

Bibbo (1987) measured the time evolution of the shear viscosity in an initially isotropic fibre suspension using the cup-and-plate rheometer. This device consists of a cylindrical cup with a force transducer on the bottom and a rotating plate on the top. The zero strain (i.e. time=0) measurements correspond to an isotropic suspension. This is because before the onset of flow the suspensions were isotropic. This was evinced by transient measurements of the shear viscosity and the normal stress in the suspension and a comparison of these values to the same transient measurements in suspensions with known orientation distributions. We shall be concerned with the shear viscosity, which is proportional to the $\sigma_{r\theta}$ component of the stress tensor, where r and θ are the radial and flow directions, respectively.

Since we compare these experimental results to the predictions of both theory and simulations for fibres in planar shear flows, the limitations of such a comparison should be mentioned. First, since the radius of the cup is of the same order as the length of the fibres, the fibres experience a non-homogeneous velocity profile. Additionally, since the radius and height of the vessel are of the same order, the 'edge effects' on the velocity profile at the inner radial wall of the vessel might not be negligible.

There is one other experimental consideration that one might initially consider to be important, but is not. If we consider a cylindrical coordinate system (z, θ, r) with its origin at the centre of the cup base, neglecting edge effects the velocity field in the rheometer is

$$\boldsymbol{v} = v_\theta = \omega R \frac{z}{H} \frac{r}{R} \tag{27}$$

where ω is the angular velocity of the rotating plate, and H and R are the height and radius of the cup, respectively. Converting to a local Cartesian coordinate system centred at any fibre where **1**, **2**, and **3** are the axial, flow, and radial directions, respectively, we see that unlike a cone-and-plate rheometer that induces shear only in the (1, 2)-plane,

$$\partial v_2(\boldsymbol{x})/\partial x_1 > 0, \quad \partial v_2(\boldsymbol{x})/\partial x_3 = 0,$$

making use of (27) we see that a cup-and-plate rheometer induces shear in both the (1,2) *and* (2,3)-planes

$$\partial v_2(\boldsymbol{x})/\partial x_1 > 0, \quad \partial v_2(\boldsymbol{x})/\partial x_3 > 0.$$

Both planes of shear can can give rise to particle stress. Owing to the linearity of the creeping flow equations, we can separate the particle stress, $\left\langle \sigma_{12}^{(P)} \right\rangle$, into the parts induced by each of the two separate flows. From (11) we see that these two parts are proportional to $\langle p_1 p_1 p_2 p_2 \rangle$ and $\langle p_1 p_2 p_2 p_3 \rangle$, respectively. Since the latter vanishes for an isotropic suspension, we see that shear in the (2,3)-plane will not contribute to

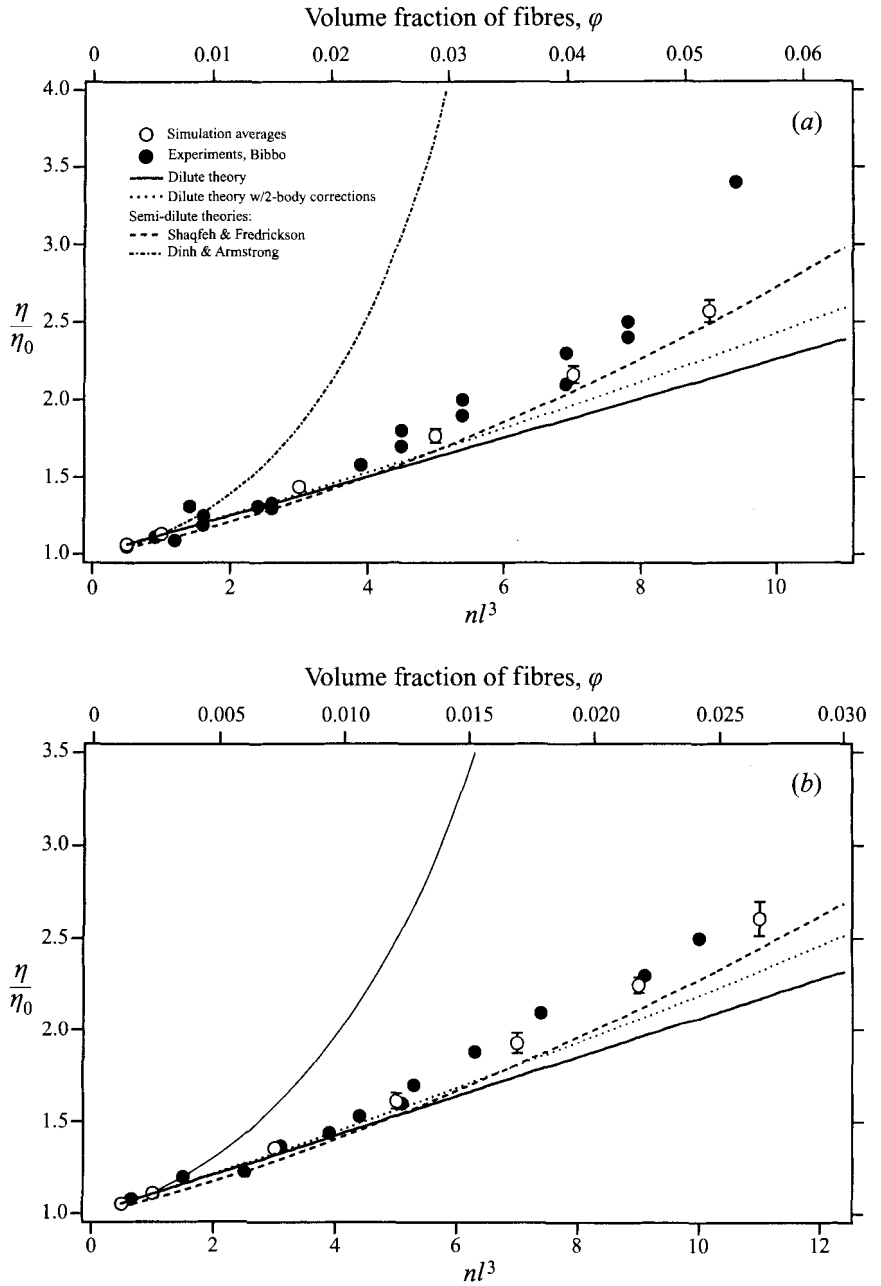

FIGURE 8. Shear viscosity of an isotropic suspension of cylindrical fibres with aspect ratio, (*a*) $A = 33$, and (*b*) $A = 51$, relative to that of the fibre-free liquid, as a function of suspension volume fraction. Shown are the experimentally determined values of Bibbo (1987), and the predictions of numerical simulations, dilute theory (with and without two-body corrections), and the semi-dilute theories of both Dinh & Armstrong (1984) and Shaqfeh & Fredrickson (1990).

σ_{12}, so comparing the experimentally measured shear viscosity to simulations having only shear in the (1, 2)-plane is valid.

In figures 8(*a*) and 8(*b*) we have plotted the experimentally determined shear viscosity of the suspension relative to that of the suspending fluid, η/η_0, for suspensions

of fibres with aspect ratios of 33 and 51, respectively. Various theoretical predictions are also shown. These theories make use of the fact that for an isotropic suspension $\langle p_i p_j \rangle = \delta_{ij}/3$ and $\langle p_i p_j p_k p_l \rangle = \left(\delta_{ij}\delta_{kl} + \delta_{ik}\delta_{jl} + \delta_{il}\delta_{jk}\right)/15$, where we have temporarily switched from Gibbs to indicial notation. For the semi-dilute theory of Shaqfeh & Fredrickson (1990), we have used $C'' = -0.6634$. This is the theoretically predicted value listed in §4 for suspensions of isotropically oriented cylinders.

Overall, we see excellent agreement between the simulations and experiments. This implies that our simulations are capturing the important physics of the system and that the effects of streamline curvature and the no-slip condition on the outer wall are small. The semi-dilute theory of Shaqfeh & Fredrickson (1990) qualitatively agrees with the simulations and experiments while quantitatively underestimating shear viscosities by about 10%. The semi-dilute theory of Dinh & Armstrong (1984) qualitatively disagrees with these results and quantitatively greatly overestimates the shear viscosities.

Only for the most concentrated suspensions in figure 8(*a*), corresponding to fibres with an aspect ratio of 33 and $nl^3 \geqslant 9$, is the agreement between experiment and simulation poor. By definition, in the semi-dilute concentration regime, the average closest approach distance between any two fibres is much greater than the characteristic fibre width. Using the results of Doi & Edwards (1989) for isotropic suspensions, this corresponds to a concentration restriction of $A/(2\pi nl^3) \gg O(1)$. However, of the different suspensions simulated in figure 8, those corresponding to the aforementioned subset have the smallest values of $A/(2\pi nl^3)$, $A/(2\pi nl^3) < 0.7$. This demonstrates that the suspension concentrations are well beyond the semi-dilute regime. Thus, there are close fibre–fibre interactions which are not captured by our slender-body theory approximation and therefore we underestimate the effective viscosity. This may have been anticipated considering that the error involved in slender-body theory in approximating fibre–fibre interactions, as shown by (5), is no longer negligible when there are many close fibre–fibre interactions.

Claeys & Brady (1993) have used Stokesian dynamics simulations to determine the shear viscosity of suspension of spheroidal particles with an aspect ratio of 50. For each of their published simulation results, holding nl^3 fixed, we have extrapolated to results for suspensions of spheroids with an aspect ratio of 51. We do this in a manner similar to the cylinder–spheroid conversion discussed earlier (although this affects the results by less than 1%). This allows us to directly compare their results to the predictions of our simulations for spheroids with aspect ratios of 51. In figure 9 we have plotted $\left\langle S_{12}^{(P)} \right\rangle$ as predicted by both our simulations, Stokesian dynamics, and the dilute theory. From (3) we see that $\left\langle S_{12}^{(P)} \right\rangle$ is the average contribution of a particle to the suspension shear viscosity. Thus, changes in $\left\langle S_{12}^{(P)} \right\rangle$ as a function of suspension volume fraction are a direct measure of the effect of fibre–fibre interactions.

In figure 9 we see that our simulations show increasing positive deviation from the dilute theory with increasing suspension concentration, while the Stokesian dynamics simulations show no such trend. Although it is difficult to draw firm conclusions owing to the scatter of the data and the limited concentration range investigated by the Stokesian dynamics simulation data, it appears that over the concentration range investigated Stokesian dynamics fails to capture the effect of fibre–fibre interactions. For similar values of nl^3, but with particles of aspect ratio 20 or less, Stokesian dynamics simulations do capture the effect of fibre–fibre interactions, apparently with increasing ability as fibre aspect ratio decreases. A probable cause for this is that

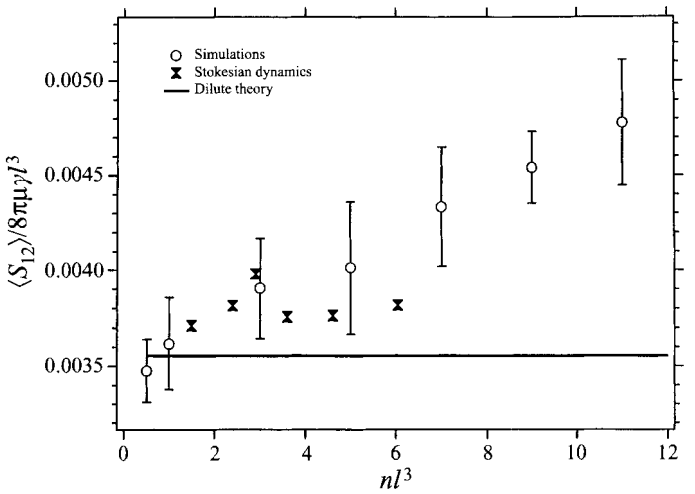

FIGURE 9. Average non-dimensionalized particle stresslet in an isotropic suspension of spheroidal fibres with aspect ratio, $A = 51$, as a function of suspension concentration. Shown are the predictions of numerical simulations, Stokesian dynamics simulations (Claeys & Brady 1993) and the dilute theory.

Stokesian dynamics effectively represents the disturbance created by a particle using the first two terms of the multipole expansion of (2) about the particle centres. It appears that with increasing particle aspect ratio, higher-order terms in the multipole expansion become increasingly important. Thus, the ability of the two-term expansion to capture fibre–fibre interactions decreases.

5.2.3. *Steady-state shear viscosity*

The steady-state fibre orientation distribution in shear flows is a function of both particle aspect ratio and suspension volume fraction. Stover, Koch & Cohen (1992) have experimentally studied this for particles having aspect ratios of 16.9 and 31.9 over similar ranges of concentrations as those investigated by Bibbo (1987). Isolated fibres in a shear flow rotate in one of a continuum of Jeffrey orbits, each denoted by an orbit constant C. The orbit in which an isolated particle finds itself is determined by its initial orientation, while the nature of the orbit is a function of the effective aspect ratio of the particle. Stover *et al.* (1992) determined that in the semi-dilute regime the time-averaged nature of the Jeffrey orbits was changed only slightly, but the steady-state distribution of orbit constants, $p(C)$, was very different from that expected for an initially isotropic suspension. The latter is well described by the anisotropic rotary diffusivity model of Rahnama *et al.* (1993)

$$p(C) = \frac{4CR}{(4C^2R+1)^{3/2}} \tag{28}$$

where $R = 2.4$ gives the best fit to experimental data. Using (28) and equations describing the Jeffrey orbits (Stover *et al.* 1992), we numerically generated suspensions having the proper steady-state orientation distributions for fibres in shear flow. Unlike our algorithms for the generation of aligned and isotropic suspensions, if a generated fibre overlapped an existing fibre, we did not reject both the centre position and orientation, but rather just generated a new centre position to complement the existing orientation. Since a fibre is more likely to avoid overlapping with a fibre of

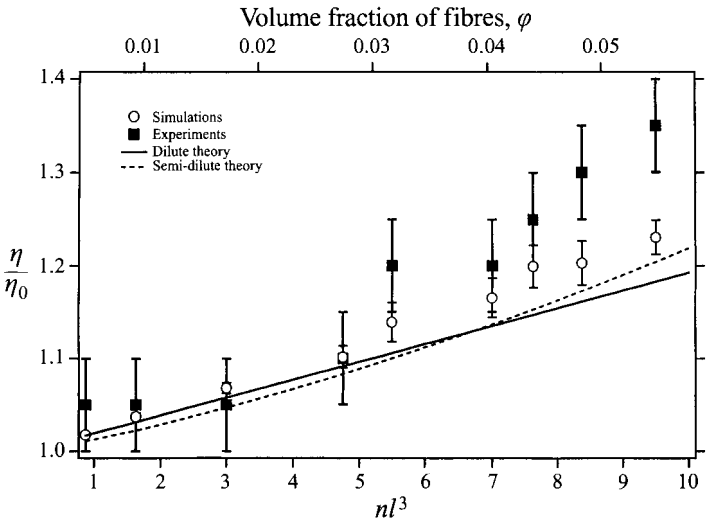

FIGURE 10. Steady-state shear viscosity of a suspension of cylindrical fibres with aspect ratio, $A = 33$, relative to that of the fibre-free liquid, as a function of suspension volume fraction. Shown are the the experimentally determined values of Bibbo (1987), and the predictions of numerical simulations, the dilute theory, and the semi-dilute theory of Shaqfeh & Fredrickson (1990).

similar orientation, and at steady state most fibres in shear are aligned in the flow direction, such a modification to our algorithm is necessary to prevent biasing our distribution.

In figure 10 we have compared our simulated results for the steady-state shear viscosity for suspensions of particles having aspect ratios of 33 to the predictions of the dilute theory and the semi-dilute theory of Shaqfeh & Fredrickson (1990). Both theories make use $\langle p_1 p_1 p_2 p_2 \rangle = 0.100$, as determined from our generated orientation distributions. For the semi-dilute theory, since the $O(1)$ constant has not been determined for this particular orientation distribution, we set it equal to zero.

In figure 10 we see fairly good agreement between simulations and experiments up to concentrations of approximately $nl^3 = 7$, above which the simulations underestimate the experimentally determined shear viscosity. Based on the previously discussed results for isotropic suspensions, and the fact that by symmetry $\langle p_1 p_1 p_2 p_3 \rangle = 0$, we believe that the curved streamlines, no-slip condition on the outer wall, and shear in the (2, 3)-plane, all present in the experimental apparatus, had a negligible effect on the shear viscosity and would not account for the discrepancy between simulation and experiments.

The likely sources of the discrepancy can be divided into two classes: those which are equally important at all suspension concentrations and those which are more important at higher concentrations. Concerning the former, there are three likely factors. First, a fibre oriented in the flow direction will make a contribution to the suspension stress tensor $O\left(\ln A/A^2\right)$ smaller than one which is not. Since the contribution to the stress of the former is driven entirely by gradients in the undisturbed velocity along the cross-sections of the fibres, it will not be captured by the slender-body theory approximation used in the simulations. For fibres in shear flow at steady state, only an $O(1/A)$ fraction of the fibres are not approximately aligned in the flow direction (Stover *et al.* 1992). Thus, the error induced by the slender-body theory approximation in calculating the steady-state shear viscosity is

$O(\ln A/A)$. This is not necessarily small for the suspensions under consideration, since $(\ln A)/A \approx 0.11$. Secondly, when comparing suspensions of the same aspect ratio, $\langle p_1 p_1 p_2 p_2 \rangle$ for our numerically generated suspensions was about 10% smaller than the experimentally determined values of Stover *et al.* (1992), due to small changes in the Jeffrey orbits induced by fibre interactions. Finally, $\langle p_1 p_1 p_2 p_2 \rangle$ in the experiments of Bibbo (1987) were probably even larger than those measured by Stover *et al.* (1992), since the effect of the aforementioned shear in the (2, 3)-plane would be to rotate fibres into the (1, 2)-plane.

It is possible to suggest a reason for the relatively poorer agreement between simulations and experiments for $nl^3 > 5$. We expect the average closest approach distance in the suspension will be between those for aligned and isotropic suspensions. However, from an analysis similar to that used by Doi & Edwards (1989), we expect the $O(1/A)$ fraction of the fibres that are not aligned in the flow direction will experience a closest approach distance of the same order as that in an isotropic suspension. Since it is these few fibres that make the dominant contribution to $\left\langle \sigma_{ij}^{(P)} \right\rangle$, and we see a decline in the agreement between simulations and experiments at approximately the same concentration as for isotropic suspensions, we suggest that the discrepancy is due to slender-body theory underestimating the effects of close fibre–fibre interactions.

6. Conclusion

For suspensions of rigid, non-Brownian fibres at zero Reynolds number, hydrodynamic fibre–fibre interactions have a negligible effect on the volume-averaged stress tensor for $nl^3 < 1$. At $nl^3 \sim O(1)$, independent of any particular fibre aspect ratio or suspension volume fraction, fibre–fibre interactions begin to enhance the stress in the suspension and it undergoes a transition to the semi-dilute regime. This transition, as well as the suspension behaviour well into the semi-dilute regime, is well predicted by dilute theories that take into account two-body interactions. In the semi-dilute regime, the dimensionless fibre disturbance screening length, χ/b, is only a function of suspension volume fraction. It is approximately the same for both aligned and isotropic suspensions, even though the latter contain many more close fibre–fibre interactions than the former. This is in qualitative agreement with the theoretical prediction of Shaqfeh & Fredrickson (1990), but disagrees with that of Dinh & Armstrong (1984). Our conclusion is supported by the experimental work of Bibbo (1987), who measured the zero-shear viscosity of an isotropic suspension. Bibbo (1987) had hypothesized that rapid alignment of the suspension caused an initially isotropic suspension to show the same screening behaviour as that expected for an aligned suspension, even at very short times. Our numerical simulations have shown that partial alignment of the suspension is not necessary for this screening behaviour to occur. The quantitative agreement between our simulations and the semi-dilute theory of Shaqfeh & Fredrickson (1990) can be greatly improved by adjusting the value of C'' in the theory to -1.25 and retaining the $O(1/\ln(1/\phi))$ term with a coefficient of 2.4. This physically corresponds to keeping classes of fibre interactions neglected by the theory. The above result is used to show that the suspension screening lengths are very similar to those in fibrous porous media having the same fibre volume fraction. This holds for both aligned and isotropic orientation distributions. We also directly verify suspension screening by studying the decay of the velocity fields created by individual Stokeslets in fibre suspensions.

Comparison of our numerical simulations to experiments and theoretical predictions for steady state shear and extensional viscosities also support the conclusion that the semi-dilute suspension screening length is independent of the fibre orientation distribution in the suspension. This conclusion is powerful since it allows one to convert knowledge of the transient fibre orientation distribution in a suspension to the transient rheological properties of the suspension. This is particularly valuable in a rapidly changing flow field where steady-state conditions are not reached since direct measurement of transient rheological properties are difficult.

Slender-body theory will faithfully capture the effect of fibre–fibre interactions on the hydrodynamic stress in an isotropic suspension for concentrations up to $nl^3 \approx A/5$, beyond which it underestimates their effect. Interestingly, although the average steady-state closest approach distance between fibres in shear flow is much larger than for those in an isotropic suspension, the few fibres that make the dominant contribution to the suspension stress experience closest approach distances that are approximately the same as those in an isotropic suspension. Consequently, in such flows the same upper concentration limit for the ability of slender-body theory to capture the full effect of fibre–fibre interactions is observed. This limit is presumably much higher in aligned suspensions, since for a given suspension concentration the average closest approach distance is much larger.

Our algorithm can easily be modified to determine the sedimentation characteristics of fibre suspensions. This is done by changing the right-hand side of (8) to specify that the net force exerted by a fibre on the fluid is equal to the gravitational body force exerted on the fibre. Monte Carlo and dynamic studies of fibre sedimentation are in progress.

The authors would like to acknowledge support for this work from both a Presidential Young Investigator Award, Grant No. CTS-90557284, to ESGS, as well as a Merck Fellowship to MBM. Computer resources (CRAY C90) were supplied by a grant from the San Diego Supercomputer Center. This material is based on work supported by Cornell University through the National Science Foundation Grant No. DDM-9212582.

Appendix. Calculations of the correction to the effective viscosity of a fibre suspension for two-body interactions

A.1. *General development*

A method for calculating expressions for the effective viscosity in a random dispersion of rigid fibres in a Newtonian fluid which accounts for multi-body interactions has been carefully presented by Shaqfeh & Fredrickson (1990). We shall refer to this publicaton for the details and only outline the mathematical steps necessary to derive the results quoted in §4 – namely the first correction to the predicted effective viscosity of a fibre solution in the dilute limit which accounts for two-body interactions.

The general theory developed by Shaqfeh & Fredrickson (1990) for the wavenumber-dependent propagator, $G_{jk}(\boldsymbol{q})$ in suspensions of randomly positioned fibres can be summarized in the following set of integral equations:

$$(\delta_{ij} - I_{im}\Sigma_{mj})G_{jk} = I_{ik}, \tag{A 1}$$

$$Q_{ij}(l\boldsymbol{q}\cdot\boldsymbol{p}, l\boldsymbol{q}'\cdot\boldsymbol{p}) = T_{ij}(l\boldsymbol{q}\cdot\boldsymbol{p}, l\boldsymbol{q}'\cdot\boldsymbol{p}) + \frac{1}{(2\pi)^3}\int \mathrm{d}\boldsymbol{k}\, T_{ik}(l\boldsymbol{q}\cdot\boldsymbol{p}, l\boldsymbol{k}\cdot\boldsymbol{p})[G_{kl}(\boldsymbol{k}) - I_{kl}(\boldsymbol{k})]Q_{lj}(l\boldsymbol{k}\cdot\boldsymbol{p}, l\boldsymbol{q}'\cdot\boldsymbol{p}), \tag{A 2}$$

$$I_{ij}(\boldsymbol{q}) = \frac{1}{\mu q^2}(\delta_{ij} - \tilde{q}_i\tilde{q}_j), \tag{A 3}$$

$$T_{ij}(l\boldsymbol{q}\cdot\boldsymbol{p}, l\boldsymbol{q}'\cdot\boldsymbol{p}) = \frac{4\pi\mu l}{\ln(2A)}F(l\boldsymbol{q}\cdot\boldsymbol{p}, l\boldsymbol{q}'\cdot\boldsymbol{p})p_ip_j + \frac{8\pi\mu l}{\ln(2A)}H(l\boldsymbol{q}\cdot\boldsymbol{p}, l\boldsymbol{q}'\cdot\boldsymbol{p})(\delta_{ij} - p_ip_j), \tag{A 4}$$

$$F(x, y) = j_0(x)j_0(y) - j_0(x - y), \tag{A 5}$$

$$H(x, y) = 3j_1(x)j_1(y) + j_0(x)j_0(y) - j_0(x - y), \tag{A 6}$$

where $\tilde{\boldsymbol{q}} = \boldsymbol{q}/q$ and where j_0 and j_1 are the spherical Bessel functions of zeroth and first order respectively. The vector $\boldsymbol{p}$ is the unit vector representing the orientation of an individual particle and the orientation distribution of the particles is only important in the calculation of the self-energy, Σ_{ij}. For aligned particles, we define the particles to be oriented in the common direction $\boldsymbol{p}$ and then

$$\Sigma_{ij} = n\, Q_{ij}(l\boldsymbol{q}\cdot\boldsymbol{p}, l\boldsymbol{q}\cdot\boldsymbol{p}) \tag{A 7}$$

where n is the number density of particles. For isotropic suspensions,

$$\Sigma_{ij} = \frac{n}{4\pi}\int \mathrm{d}\boldsymbol{p} Q_{ij}(l\boldsymbol{q}\cdot\boldsymbol{p}, l\boldsymbol{q}\cdot\boldsymbol{p}). \tag{A 8}$$

Finally, since $T_{ij}(l\boldsymbol{q}\cdot\boldsymbol{p}, l\boldsymbol{q}'\cdot\boldsymbol{p})$ is a symmetric tensor described in terms of the single unit vector $\boldsymbol{p}$, we can also decompose $Q_{ij}(l\boldsymbol{q}\cdot\boldsymbol{p}, l\boldsymbol{q}'\cdot\boldsymbol{p})$ into Q_1 and Q_2 through the expression

$$Q_{ij}(l\boldsymbol{q}\cdot\boldsymbol{p}, l\boldsymbol{q}'\cdot\boldsymbol{p}) = Q_1(l\boldsymbol{q}\cdot\boldsymbol{p}, l\boldsymbol{q}'\cdot\boldsymbol{p})p_ip_j + Q_2(l\boldsymbol{q}\cdot\boldsymbol{p}, l\boldsymbol{q}'\cdot\boldsymbol{p})(\delta_{ij} - p_ip_j). \tag{A 9}$$

A.2. *Aligned fibres*

As demonstrated by Shaqfeh & Fredrickson (1990), the expression for μ^{fibre} for aligned suspensions can be determined from the following formula:

$$\mu^{fibre} = -\lim_{\xi\to 0}\frac{nl^2}{2}\frac{\mathrm{d}^2Q_1(\xi, \xi)}{\mathrm{d}\xi^2}, \tag{A 10}$$

where $\xi = l\boldsymbol{q}\cdot\boldsymbol{p}$. Thus we need only concentrate on the asymptotic form for $Q_1(\xi, \xi)$ in the limit $nl^3 \to 0$ to determine the dilute form for μ^{fibre}.

In (A2) for $Q_{ij}(l\boldsymbol{q}\cdot\boldsymbol{p}, l\boldsymbol{q}'\cdot\boldsymbol{p})$ the first term on the right-hand side is the transfer matrix in the absence of particle interactions $T_{ij}(l\boldsymbol{q}\cdot\boldsymbol{p}, l\boldsymbol{q}'\cdot\boldsymbol{p})$ and the second integral term represents the multi-body interactions and their effect on transfer. To take into account the first reflection interactions on this transfer we need only consider the first iterate of this equation in the limit of $nl^3 \to 0$ (with the limit taken assuming $q \sim O(1/l)$). This gives the result

$$Q_{ij}(l\boldsymbol{q}\cdot\boldsymbol{p}, l\boldsymbol{q}'\cdot\boldsymbol{p}) = T_{ij}(l\boldsymbol{q}\cdot\boldsymbol{p}, l\boldsymbol{q}'\cdot\boldsymbol{p}) + \frac{1}{(2\pi)^3}\int \mathrm{d}\boldsymbol{k}\, T_{ik}(l\boldsymbol{q}\cdot\boldsymbol{p}, l\boldsymbol{k}\cdot\boldsymbol{p})[G'_{kl}(\boldsymbol{k})]T_{lj}(l\boldsymbol{k}\cdot\boldsymbol{p}, l\boldsymbol{q}'\cdot\boldsymbol{p}), \tag{A 11}$$

where $G'_{kl} = \lim_{nl^3\to 0}[G_{kl} - I_{kl}]$ and where

$$\Sigma_{ij} = nT_{ij}(l\boldsymbol{q}\cdot\boldsymbol{p}, l\boldsymbol{q}\cdot\boldsymbol{p}). \tag{A 12}$$

We need only determine Q_1 in order to find μ_{fibre}, so we consider the somewhat

reduced integral relation

$$Q_1(\xi,\xi) = \frac{4\pi\mu l}{\ln(2A)}F(\xi,\xi) + \frac{1}{(2\pi)^3}\int \mathrm{d}\boldsymbol{k}[\frac{4\pi\mu l}{\ln(2A)}]^2 F(\xi, l\boldsymbol{k}\cdot\boldsymbol{p})p_k G'_{kl}p_l F(l\boldsymbol{k}\cdot\boldsymbol{p},\xi). \quad (A\,13)$$

Noting that

$$\lim_{\xi\to 0}F(\xi, l\boldsymbol{k}\cdot\boldsymbol{p}) \to -\xi j_1(l\boldsymbol{k}\cdot\boldsymbol{p}) \quad (A\,14)$$

and, similarly

$$\lim_{\xi\to 0}F(l\boldsymbol{k}\cdot\boldsymbol{p},\xi) \to -\xi j_1(l\boldsymbol{k}\cdot\boldsymbol{p}) \quad (A\,15)$$

we can substitute our integral expression for $Q_1(\xi,\xi)$ into the definition of μ^{fibre} and using the limits defined above, we obtain

$$\mu^{fibre} = \frac{4\pi\mu n l^3}{3\ln(2A)} - \frac{2nl^3\mu^2 l}{\pi\ln(2A)}\int \mathrm{d}\boldsymbol{k} j_1^2(l\boldsymbol{k}\cdot\boldsymbol{p})p_k G'_{kl}p_l(\boldsymbol{k}) \quad (A\,16)$$

where the first term on the right-hand side is the one-particle result and the second term is the correction due to two-particle interactions. Note that this method rigorously takes into account all first reflection interactions on the value of μ^{fibre}. These give the leading order correction in the dual limit $nl^3 \to 0$ and $A \gg 1$ (or more precisely, $1/\ln(2A) \ll 1$). To complete the derivation we need only determine $p_k G'_{kl}p_l(\boldsymbol{k})$. If we examine the Green's function calculated by Shaqfeh & Fredrickson (1990) for aligned fibre suspensions, then it can be shown that

$$p_k G'_{kl}p_l(\boldsymbol{k}) \approx n\frac{4\pi\mu l}{\ln(2A)}\frac{F(kx,kx)(1-x^2)^2 + 2H(kx,kx)x^2(1-x^2)}{\mu^2 k^4} \quad (A\,17)$$

where $x \equiv l\boldsymbol{k}\cdot\boldsymbol{p}$. Substituting this result back into the integral for μ_{fibre} and manipulating gives

$$\mu_{fibre} = \frac{4\pi\mu n l^3}{3\ln(2A)} + \frac{32\pi(nl^3)^2}{\ln^3(2A)} \times J, \quad (A\,18)$$

$$J = \int_0^\infty \mathrm{d}k \int_0^1 \mathrm{d}x \frac{[1-j_0^2(kx)]j_1^2(kx)(1-x^2)^2}{k^2} + \frac{2j_1^2(kx)[1-j_0^2(kx)-3j_1^2(kx)]x^2(1-x^2)}{k^2}. \quad (A\,19)$$

The integral J was completed numerically and found to have the value $J = 0.01718$. With this numerical result we obtain the quoted value of $Q^{2-body}_{Aligned}$ found in §4.2.

A.3. *Isotropic suspensions*

Interestingly the equation for μ^{fibre} derived above in terms of G'_{kl} remains the same if the suspension is isotropic, but, of course, the value of G'_{kl} changes. This equation physically represents the fact that the dipole or stresslet correction on a given fibre occurs due to the average reflected field from the surrounding fibres. Thus, the method of calculating this change does not depend on the orientation distribution, but the form of the reflected field does.

Turning then to the calculation of G'_{kl} for isotropic suspensions, we have that the self-energy no longer depends on any preferred direction, and takes the form

$$\Sigma_{ij} = A(q)\tilde{q}_i\tilde{q}_j + B(q)[\delta_{ij} - \tilde{q}_i\tilde{q}_j]. \quad (A\,20)$$

One can easily relate $B(q)$ to $Q_1(\xi,\xi)$ and $Q_2(\xi,\xi)$:

$$B = \frac{n}{4}\int_{-1}^{1} \mathrm{d}\xi Q_1(\xi,\xi)(1-\xi^2) + Q_2(\xi,\xi)(1+\xi^2). \quad (A\,21)$$

Referring to Shaqfeh & Fredrickson (1990), we have that

$$G'_{kl}(\boldsymbol{k}) \approx \frac{B(k)}{\mu^2 k^4}[\delta_{kl} - \tilde{k}_k \tilde{k}_l] \tag{A 22}$$

where $B(k)$ can be approximated in the dilute limit as

$$B(k) \approx \frac{\pi \mu n l}{\ln(2A)} \int_{-1}^{1} \mathrm{d}x F(kx, kx)(1 - x^2) + 2H(kx, kx)(1 + x^2). \tag{A 23}$$

Substituting our expression for G'_{kl} back into the integral for μ^{fibre} gives (after some manipulation)

$$\mu^{fibre} = \frac{4\pi \mu n l^3}{3 \ln(2A)} + \frac{4\pi (nl^3)^2}{\ln^3(2A)} \times J \tag{A 24}$$

where

$$J = \int_0^\infty \mathrm{d}k \int_0^1 \mathrm{d}y \int_0^1 \mathrm{d}x\, 4\, \frac{j_1^2(ky)(1 - j_0^2(kx))(1 - x^2)(1 - y^2)}{k^2} + 8 \frac{2 j_1^2(ky)(1 - j_0^2(kx) - 3 j_1^2(kx))(1 - y^2)(1 + x^2)}{k^2}. \tag{A 25}$$

Note that the correction term (the second term in the expression for μ^{fibre}) is exactly a factor of 3 larger than that calculated by Shaqfeh & Fredrickson (1990). The integral J was numerically calculated by Shaqfeh and Fredrickson to have the value $J = 0.1518$ (this was verified again in this work). Substituting this numerical result into our expression for μ^{fibre} reproduces the value of $Q^{2\text{-}body}_{Isotropic}$ quoted in §4.2.

Note added in proof

For the simulations presented in §5.1.4, $\boldsymbol{H}_P(\boldsymbol{x})$ was evaluated using the grid point interpolation algorithm developed by Mackaplow (1995). This consists of first pre-evaluating $\boldsymbol{H}_P(\boldsymbol{x})$ at 10^6 non-uniformly spaced points in 3-space. Then, any other values of $\boldsymbol{H}_P(\boldsymbol{x})$ required for the simulations are determined from these. This algorithm reduced the computational effort required for evaluating $\boldsymbol{H}_P(\boldsymbol{x})$ 300 fold, while introducing only a mean error of only 3% into each of the tensor elements.

REFERENCES

BATCHELOR, G. K. 1970 Slender-body theory for particles of arbitrary cross-section in Stokes flow. *J. Fluid Mech.* **44**, 419–440.

BATCHELOR, G. K. 1971 The stress generated in a non-dilute suspension of elongated particles by pure straining motion. *J. Fluid Mech.* **46**, 813–829.

BIBBO, M. A. 1987 Rheology of semiconcentrated fibre suspensions. PhD Thesis, Massachusetts Institute of Technology.

BONNECAZE, R. T. & BRADY, J. F. 1990 A method of determining the effective conductivity of dispersions of particles. *Proc. R. Soc. Lond.* A **430**, 285–313.

BRINKMAN, H. C. 1947 A calculation of the viscous force exerted by a flowing fluid on a dense swarm of particles. *Appl. Sci. Res.* A **1**, 27.

CLAEYS, I. L. & BRADY, J. F. 1989 Lubrication singularities of the grand resistance tensor for two arbitrary particles. *PhysicoChem. Hydrodyn.* **11**, 261-293.

CLAEYS, I. L. & BRADY, J. F. 1993 The dynamics of prolate spheroids in Stokes flow. Part 2. Statistically homogeneous dispersions. *J. Fluid Mech.* **251**, 443–477.

DINH, S. M. & ARMSTRONG, R. C. 1984 A rheological equation of state for semi-concentrated fibre suspension. *J. Rheol.* **28**, 207–227.

DOI, M. & EDWARDS, S. F. 1989 *The Theory of Polymer Dynamics*, p. 330. Oxford University Press.

DURLOFSKY, L. & BRADY, J. F. 1987 Analysis of the Brinkman equation as a model for flow in porous media. *Phys. Fluids* **30**, 3329–3341.

EWALD, P. P. 1921 Die Berechnung optischer und elektrostatischer Gitterpotentiale. *Ann. Phys.* **64**, 253–287.

FREDRICKSON, G. H. & SHAQFEH, E. S. G. 1989 Heat and mass transport in composites of aligned slender fibres. *Phys. Fluids* A **1**, 3–20.

HARLEN, O. G., SUNDARARAJAKUMAR, R. R. & KOCH, D. L. 1995 Numerical simulations of a sphere settling through a suspension of neutrally buoyant fibres. Submitted to *J. Fluid Mech.*

HARRIS, J. B. & PITTMAN, J. F. T. 1976 Alignment of slender rod-like particles in suspension using converging flows. *Trans. Instn Chem. Engrs* **54**, 73–83.

HASIMOTO, H. 1959 On the periodic fundamental solutions of the Stokes equations and their application to viscous flow past a cubic array of spheres. *J. Fluid Mech.* **5**, 317–328.

HOWELLS, I. D. 1974 Drag due to the motion of a Newtonian fluid through a sparse random array of small rigid objects. *J. Fluid. Mech.* **64**, 449–475.

JACKSON, G. W. & JAMES, D. F. 1986 The permeability of fibrous porous media. *Can. J. Chem. Engng* **64**, 364–373.

KOCH, D. L. & BRADY, J. F. 1986 The effective diffusivity of fibrous porous media. *AIChE J.* **32**, 575–591.

LADYZHENSKAYA, O. A. 1963 *The Mathematical Theory of Viscous Incompressible Flow.* Gordon & Breach.

MACKAPLOW, M. B. 1995 A study of the transport properties and sedimentation characteristics of fibre suspensions. PhD Thesis, Stanford University.

MACKAPLOW, M. B., SHAQFEH, E. S. G. & SCHIEK, R. L. 1994 A numerical study of heat and mass transport in fibre suspensions. *Proc. R. Soc. Lond.* A **447**, 77–110.

MEWIS, J. & METZNER, A. B. 1974 The rheological properties of suspensions of fibres in Newtonian fluids subject to extensional deformations. *J. Fluid Mech* **62**, 593–600.

MILLIKEN, W. J., GOTTLIEB, M., GRAHAM, A. L., MONDY, L. A. & POWELL, R. J. 1989 The viscosity-volume fraction relation for suspensions of rod-like particles by falling-ball rheometry. *J. Fluid Mech* **202**, 217–232.

O'BRIEN, R. W. 1979 A method for the calculation of the effective transport properties of suspensions of interacting particles. *J. Fluid Mech* **91**, 17–39.

PRESS, W. H., FLANNERY, B. P., TEUKOLSKY, S. A. & VETTERLING, W. T. 1990 *Numerical Recipes: The Art of Scientific Computing (FORTRAN Version)*, p. 292. Cambridge University Press

PITTMAN, J. F. T. & BAYRAM, J. 1990 Extensional flow of polydisperse fibre suspensions in free-falling liquid jets. *Intl J. Multiphase Flow* **16**, 545–559.

RAHNAMA, M., KOCH, D. L., ISO, Y. & COHEN, C. 1993 Hydrodynamic, translational diffusion in fibre suspensions subject to simple shear flow. *Phys. Fluids* A **5**, 849–862.

SANDSTROM, C. R. & TUCKER III, C. L. 1993 A theory for concentrated fibre suspensions with strong fibre-fibre interactions. *Makromol. Chem., Macromol. Symp.* **68**, 291–300.

SHAQFEH, E. S. G. & FREDRICKSON, G. H. 1990 The hydrodynamic stress in a suspension of rods. *Phys. Fluids* A **2**, 7–24.

SHAQFEH, E. S. G. & KOCH, D. L. 1990 Orientational dispersion of fibres in extensional flows. *Phys. Fluids* A **2**, 1077–1093.

STOVER, C. A., KOCH, D. L. & COHEN, C. 1992 Observations of fibre orientation in simple shear flow of semi-dilute suspensions. *J. Fluid Mech.* **238**, 277–296.

WEINBERGER, C. B. 1970 PhD thesis, University of Michigan.

YOUNGREN, G. K. & ACRIVOS, A. 1975 Stokes flow past a particle of arbitrary shape: a numerical method of solution. *J. Fluid Mech.* **69**, 377–403.